

# Optical Theorem, Crossing Property and Derivative Dispersion Relations: Implications on the Asymptotic Behavior of $\sigma_{\text{tot}}(s)$ and $\rho(s)$

S. D. Campos\*

*Applied Mathematics Laboratory-CCTS/DFQM,  
Federal University of São Carlos,  
Sorocaba CEP 18052-780, Brazil*

V. A. Okorokov†

*National Research Nuclear University MEPhI (Moscow Engineering  
Physics Institute), Kashirskoe highway 31, 115409 Moscow, Russia  
(Dated: August 23, 2022)*

In this paper, one presents some results concerning the behavior of the total cross section and  $\rho$ -parameter at asymptotic energies in proton–proton ( $pp$ ) and antiproton–proton ( $\bar{p}p$ ) collisions. For this intent, we consider three of the main theoretical results in high energy physics: the crossing property, the derivative dispersion relation, and the optical theorem. The use of such machinery allows the analytic formulas for wide set of the measured global scattering parameters and some important relations between them. The suggested parameterizations approximate simultaneously the energy dependence for total cross section and  $\rho$ -parameter for  $pp$  and  $\bar{p}p$  with statistically acceptable quality in multi-TeV region. Also the qualitative description is obtained for important interrelations, namely difference, sum and ratio of the antiparticle–particle and particle–particle total cross sections. Despite the reduced number of experimental data for the total cross section and  $\rho$ -parameter in TeV-scale, which turns any prediction for the beginning of the asymptotic domain a hard task, the fitting procedures indicates that asymptotia lies in the energy range 25.5–130 TeV. Moreover, in the asymptotic regime, one obtains  $\alpha_{\mathbb{P}} = 1$ . Detailed quantitative study of energy behavior of measured scattering parameters and their combinations in ultra-high energy domain indicates that the scenario with the generalized formulation of the Pomeranchuk theorem is more favorable with respect to the original formulation of this theorem.

PACS numbers: 13.85.Dz

## I. INTRODUCTION

The absence of a rigorous formalism able to predict elastic and diffractive processes, the so-called soft scattering states, turns soft interactions into a great challenge for quantum chromodynamics (QCD). As a complementary difficulty, the use of asymptotic theorems in high energy physics are also a hard matter since there is no indication when they must start to be applied, i.e. where the asymptotia should begins. Furthermore, they also emerge in different contexts in the  $S$ -matrix, a pre-QCD formalism.

There are a few of the rigorous theorems which are crucially important for high energy physics, and, especially, for the asymptotic energy domain. In the present work, we analyze two of the most outstanding among them, namely Froissart–Martin bound and Pomeranchuk theorem, both concerning particle–particle and antiparticle–particle total cross sections ( $\sigma_{\text{tot}}$ ), a forward quantity (zero transferred momentum).

Probably, the so-called Froissart–Martin bound [1–4] and its recent modification [5], is the most relevant asymptotic bound in forward high energy scattering, since it furnishes some kind of physical limit to the total cross section rise as the collision energy grows. This theoretical result is the effect of the analyticity of elastic scattering amplitude and rigorous consequence of the most general properties of quantum field theory (QFT), namely, causality, unitarity, and the polynomial boundness [2, 3]. This asymptotic bound is pre-QCD and works, in fact, as a general parameterization for several models concerning the rise of  $\sigma_{\text{tot}}$ . In the QCD framework, there is no formal derivation of this bound from the first principles unless the functional integral approach [6]. However, the absence of a non-perturbative QCD corroboration does not contradict the robustness of such inequality.

Another interesting forward asymptotic result is given by the Pomeranchuk theorem [7], and it concerns the difference between  $\sigma_{\text{tot}}$  for particle–particle and antiparticle–particle. As well-known, this theorem is the consequence of

---

\*Electronic address: sergiode@ufscar.br

†Electronic address: VAOkorokov@mephi.ru; Okorokov@bnl.gov

the crossing property and an effect of the analyticity of the scattering amplitude. The Pomeranchuk theorem predicts that, for sufficiently high energies, the difference between these total cross sections should vanish. The general belief about this result imposes the need for a particle exchange as responsible for the vanishing difference as the collision energy grows. This particle is called the leading Regge pole [8], or Pomeron for short, and it does not differentiate particle from antiparticle since it possesses the vacuum quantum numbers. The usual picture where the Pomeron is viewed as a pair of gluons is due to Low and Nussinov [9, 10]. Despite the huge amount of experimental data, there is no evidence for the Pomeron up to the present-day energies.

In the phenomenological context, the above two theorems remain as fundamental to impose constraints on the rise of  $\sigma_{\text{tot}}$  as the collision energy grows. However, they do not stand alone when we talk about forward quantities. The optical theorem is a remarkable result connecting the total cross section and the imaginary part of the forward scattering amplitude [11]. Moreover, the derivative dispersion relations (DDR) can be used to connect the imaginary part of the forward scattering amplitude with the real part [12]. Thus, at least in the forward collision context, a whole scattering amplitude can be constructed based on few theoretical results.

It should be stressed that if we assume that crossing property is valid, despite its lack of theoretical and experimental evidence, then we can obtain the forward scattering amplitude for particle–particle events from the forward scattering amplitude for antiparticle–particle scattering (and vice-versa).

In the present work, one uses the crossing property, the DDR, and the optical theorem to obtain some theoretical results on the rise of  $\sigma_{\text{tot}}$ . In particular, based on these results, one presents a simple fitting model for the proton–proton ( $pp$ ) and antiproton–proton ( $\bar{p}p$ ) total cross sections. Our results indicate that, asymptotically, a Pomeron intercept  $\alpha_{\mathbb{P}} = 1$ . Moreover, one also estimates the energy range where the asymptotic regime should begin.

The paper is organized as follows. In section II, some considerations are discussed about the total cross section. Section III contains a detailed description of experimental databases considered in the paper and corresponding procedures for approximation. Section IV presents the parameters obtained in the fitting procedure. Discussion and projections for some global scattering parameters are in the Section V. Section VI contains conclusions and final remarks.

## II. ASYMPTOTIC BEHAVIOR OF TOTAL CROSS SECTION AND $\rho$ -PARAMETER

As is well-known, the crossing property has never been proven (see, for instance, [13]), but in general, based on it, one postulates that scattering amplitudes can be analytically continued between the different channels of the collision process. Then, one assumes that it is possible to write the scattering amplitude in terms of auxiliary even (+) and odd (−) amplitudes as

$$2f_{\pm}(s, t) = F_{pp}(s, t) \pm F_{\bar{p}p}(s, t), \quad (1)$$

where  $f_{\pm}(s, t) = \text{Re}f_{\pm}(s, t) + i\text{Im}f_{\pm}(s, t)$  are the crossing amplitudes, and  $F_{pp}(s, t)$  and  $F_{\bar{p}p}(s, t)$  are the complex-valued scattering amplitudes for  $pp$  and  $\bar{p}p$  processes. As usual,  $s$  stands for the square of collision energy and  $-t$  for the square of transferred momentum, both in the center-of-mass system.

Based on the above definition, the DDR can be written, up to the first-order approximation, for the odd and even amplitudes (1) in the forward direction ( $t = 0$ ) as [12, 14]

$$\frac{\text{Re}f_{+}(s)}{s} = \frac{k}{s} + \left[ \frac{\pi}{2} \frac{d}{d \ln s} \right] \frac{\text{Im}f_{+}(s)}{s}, \quad (2a)$$

$$\frac{\text{Re}f_{-}(s)}{s} = \left[ \frac{\pi}{2} \left( 1 + \frac{d}{d \ln s} \right) \right] \frac{\text{Im}f_{-}(s)}{s}, \quad (2b)$$

where  $f_{\pm}(s, 0) \equiv f_{\pm}(s)$ , and  $k$  is the subtraction constant. Without loss of generality, one adopts  $k = 0$  since the influence of such parameter is restricted to the low energy domain [8]. Notice the addition of high-order derivative terms in equations (2) may turn this representation more sensitive to describe high-energy experimental data. Taking into account the representation (1), and DDR (2), the simple scheme below summarizes the use of such odd and even amplitudes

$$\text{Im}F_{xp}(s) \longrightarrow \text{Im}f_{\pm}(s) \longrightarrow \text{Re}f_{\pm}(s) \longrightarrow \text{Re}F_{xp}(s),$$

where  $x = p, \bar{p}$ . This scheme reveals the importance of phenomenological information (the input) about the imaginary part of the forward scattering amplitude. Furthermore, through the optical theorem, the forward imaginary part can

be used to define the total cross section behavior. As is well-known, the optical theorem lives in the core of high energy physics, and it was proved to be valid for all energies and scattering angles [11], being written as

$$\sigma_{\text{tot}}^{xp}(s) = \text{Im}F_{xp}(s)/s. \quad (3)$$

The optical theorem (3), as well as the DDR (2), can be used to obtain the two following results concerning the behavior of  $\sigma_{\text{tot}}$  as  $s$  grows

$$\frac{d\Delta_{\text{tot}}(s)}{d\ln s} = \frac{2}{s} \left\{ \frac{1}{\pi} [\text{Re}F_{\bar{p}p}(s) - \text{Re}F_{pp}(s)] + \text{Im}f_-(s) \right\}, \quad (4a)$$

$$\frac{d\Sigma_{\text{tot}}(s)}{d\ln s} = \frac{2}{\pi s} [\text{Re}F_{\bar{p}p}(s) + \text{Re}F_{pp}(s)] \quad (4b)$$

where the difference and sum of  $pp$  and  $\bar{p}p$  total cross sections are written, respectively, as

$$\Delta_{\text{tot}}(s) \equiv \sigma_{\text{tot}}^{\bar{p}p}(s) - \sigma_{\text{tot}}^{pp}(s), \quad (5a)$$

$$\Sigma_{\text{tot}}(s) \equiv \sigma_{\text{tot}}^{\bar{p}p}(s) + \sigma_{\text{tot}}^{pp}(s). \quad (5b)$$

One can note the relation (4a) implies the independence of  $\Delta_{\text{tot}}(s)$  and  $\text{Im}f_-(s)$  on each other for further calculations which in turn is based on the above definitions of the parameters  $\Delta_{\text{tot}}(s)$  and  $\Sigma_{\text{tot}}(s)$  via only measuring quantities ( $\sigma_{\text{tot}}^{xp}$ ) without possible consequent transition to the imaginary parts of amplitudes. Of course, the experimentally measured  $pp$  and  $\bar{p}p$  total cross sections can be written using the above results as follow:

$$2\sigma_{\text{tot}}^{\bar{p}p}(s) = \Sigma_{\text{tot}}(s) + \Delta_{\text{tot}}(s), \quad (6a)$$

$$2\sigma_{\text{tot}}^{pp}(s) = \Sigma_{\text{tot}}(s) - \Delta_{\text{tot}}(s). \quad (6b)$$

Equations (4) can be analyzed taking into account some expected particularities for  $\text{Im}F_{xp}(s)$  and  $\text{Re}F_{xp}(s)$ . First of all, at very high energies one expects, from the phenomenological point of view, that

$$\text{Re}F_{xp}(s) \ll \text{Im}F_{xp}(s), \quad (7)$$

which means an *almost* complete absorptive scattering. On the other hand, the Froissart–Martin bound states that for  $pp$  and  $\bar{p}p$  forward collision, the total cross section obeys the inequality

$$\sigma_{\text{tot}}(s)|_{s \rightarrow \infty} \leq C \ln^2 \varepsilon, \quad (8)$$

where  $C$  is a constant,  $\varepsilon \equiv s/s_0$  and  $s_0$  is some fixed scale which is, in general, unspecified. The scale can be chosen to hadronic particles as the reasonable one  $s_0 = 1 \text{ GeV}^2$  [15]. At this choice of  $s_0$ , the axiomatic quantum field theory (AQFT) resulted in  $C = \pi/m_\pi^2 \approx 62.8 \text{ mb}$  [3, 4] while the twice smaller value  $\pi/2m_\pi^2 \approx 31.4 \text{ mb}$  was recent derived [5] with  $m_\pi$  being the charged pion mass [16]. It is well-known that bound (8) cannot be improved using only analyticity in the momentum transfer, unitarity, and boundedness by a polynomial in  $s$ , even if oscillations were allowed [17].

The theoretical results (3) and (8) allow the construction of a wide room to accommodate several functional forms of  $\text{Re}F_{xp}(s)$  which satisfies the phenomenological condition (7). The simplest suggestion among them is to choose a sufficiently small constant (which can always be done), in order to satisfy relation (7) at asymptotically high energies. Then, one can suppose from some energy  $\sqrt{s_a}$ , and in consideration of the onset of the asymptotic region in the elastic scattering case that: (i)  $\text{Re}F_{xp}(s) = 0$ , or (ii)  $\text{Re}F_{xp}(s)/s = c_x \neq 0$  is a small real number depending on  $x$ , or (iii)  $\text{Re}F_{xp}(s)/s = c \neq 0$ , where  $c$  is a small real number.

Taking into account the assumption (i) in (2b), one obtains a simple expression for the odd auxiliary function

$$\text{Im}f_-(s)/s = a_1/\varepsilon, \quad (9)$$

where  $a_1$  is an integration constant and, for the sake of simplicity, hereafter one adopts the lower limit of integration as  $s_0$ . Using result (9) and assumption (i), then from (4a) one has

$$\Delta_{\text{tot}}(s) = -2a_1/\varepsilon. \quad (10)$$

Notice that the sign of  $a_1$  determines which of both total cross sections rise faster as  $s$  grows. For example, if  $a_1 < 0$ , one has  $\sigma_{\text{tot}}^{\bar{p}p}(s) \gtrsim \sigma_{\text{tot}}^{pp}(s)$ , for asymptotic energies.

At the end of the 1950s, the general belief assure that total cross section decreases with the increasing collision energy, as shown by the experimental data. As is well-known, this conviction was only modified with the Intersecting Storage Rings (ISR) measurement of the  $pp$  total cross section done in 1973 showing the increase of  $\sigma_{\text{tot}}^{pp}(s)$  with energy.

Possibly, the first theoretical result using the asymptotic condition as a way to obtain some useful ground in high energy physics is the Pomeranchuk theorem [7]. The original version assumes that if the forward elastic scattering amplitude grows slower than  $s$ , then the difference between  $\bar{p}p$  and  $pp$  total cross sections tend to zero, as  $s \rightarrow \infty$

$$\Delta_{\text{tot}}(s) \rightarrow 0, \text{ if } |F(s)| < s. \quad (11)$$

The Pomeranchuk proof uses dispersion relations and some additional intuitive assumptions, removed in other versions of the Pomeranchuk result, usually written as [18–20]

$$R_{\text{tot}}^{\bar{p}/p}(s) \equiv \sigma_{\text{tot}}^{\bar{p}p}(s)/\sigma_{\text{tot}}^{pp}(s) \rightarrow 1, \text{ if } s \rightarrow \infty, \quad (12)$$

which, one stresses, is not the same result expressed by (11).

In the light of the present assumption (i), when  $s \rightarrow \infty$  the result (10) vanishes asymptotically, corroborating the Pomeranchuk theorem. In contrast, if we use the assumption (ii), it implies in the following result

$$[\text{Re}F_{\bar{p}p}(s) - \text{Re}F_{pp}(s)]/s = c_{\bar{p}} - c_p. \quad (13)$$

In this case, one has from (2b)

$$\text{Im}f_-(s)/s = (c_{\bar{p}} - c_p)/\pi + a_2/\varepsilon. \quad (14)$$

where  $a_2 \neq 0$  is an integration constant. Using above result, then the difference between the total cross sections is written as

$$\Delta_{\text{tot}}(s) = [4(c_{\bar{p}} - c_p)/\pi] \ln \varepsilon - 2a_2/\varepsilon, \quad (15)$$

which does not corroborate the Pomeranchuk theorem unless  $c_{\bar{p}} = c_p$ . The last assumption (iii) implies  $c_{\bar{p}} = c_p = c$ , and, in this case, the difference is null

$$\text{Re}F_{\bar{p}p}(s) - \text{Re}F_{pp}(s) = 0. \quad (16)$$

The above result implies an asymptotic behavior for the total cross section similar to (10). From this simple analysis, it is possible to conclude that  $\text{Re}F_{xp}(s) = 0$  or  $\text{Re}F_{xp}(s)/s = c$  at high energies since both results corroborate with the Pomeranchuk theorem.

Equation (4b) can also provide physical information on the behavior of  $\Sigma_{\text{tot}}(s)$ . Taking into account assumption (i), then from some  $s_a$ , one has

$$\Sigma_{\text{tot}}(s) = a_0, \quad (17)$$

where  $a_0$  is a real constant. It is important to stress this result does not violate any theorem in high energy physics, and it seems to indicate the existence of some taming mechanism (for example, the mini-jet [21]) to the rise of  $\sigma_{\text{tot}}(s)$  as  $s$  grows.

In contrast, for a non-null real part given by assumption (ii), one obtains

$$\Sigma_{\text{tot}}(s) = [2(c_{\bar{p}} + c_p)/\pi] \ln \varepsilon, \quad (18)$$

which notably reveals that in the asymptotic limit the sum of the cross sections follow the logarithm of the collision energy, i.e. with a Pomeron intercept  $\alpha_{\mathbb{P}} = 1$ . Considering assumption (iii), one can derive a similar result

$$\Sigma_{\text{tot}}(s) = (4c/\pi) \ln \varepsilon. \quad (19)$$

It is unnecessary to say that results (18) and (19) does not violate the Froissart–Martin theorem (8) even in its modified version [5].

For clarity, all the above results are summarized in Table I. From this table, one observes that for (i), although  $\Delta_{\text{tot}}(s)$  obeys the Pomeranchuk theorem, the sum  $\Sigma_{\text{tot}}(s)$  seems to not correspond to the behavior shown by the experimental data, at least in the present-day energies. For the results expressed by (ii), on the other hand, one has

TABLE I: Summary of the theoretical results obtained assuming the asymptotic condition  $s \rightarrow \infty$ .

Assumption	$\text{Re}F_{xp}(s)/s$	$\text{Im}f_-(s)/s$	$\Delta_{\text{tot}}(s)$	$\Sigma_{\text{tot}}(s)$
(i)	0	$a_1/\varepsilon$	$-2a_1/\varepsilon$	$a_0$
(ii)	$c_x$	$(c_{\bar{p}} - c_p)/\pi + a_2/\varepsilon$	$[4(c_{\bar{p}} - c_p)/\pi] \ln \varepsilon - 2a_2/\varepsilon$	$[2(c_{\bar{p}} + c_p)/\pi] \ln \varepsilon$
(iii)	$c$	$a_1/\varepsilon$	$-2a_1/\varepsilon$	$(4c/\pi) \ln \varepsilon$

that  $\Delta_{\text{tot}}(s)$  does not obey the Pomeranchuk theorem, unless  $c_{\bar{p}} = c_p$ . The last results given by (iii) seems to be reasonable under the lights of the experimental data, representing a Pomeron intercept  $\alpha_{\mathbb{P}} = 1$  [8].

Therefore, one may conclude that  $pp$  and  $\bar{p}p$  real part of the forward elastic amplitude are null above some energy  $\sqrt{s_a}$  or that they are equals. Both conclusions preserve the Pomeranchuk theorem as well as the Froissart–Martin bound. However, they lead to different asymptotic behaviors for  $\Sigma_{\text{tot}}(s)$ , which represents a puzzle that apparently cannot be solved at present-day energy. It is important to stress that considering the results shown in Table I as well as (6), one can obtain analytic expressions for experimentally measured quantities  $\sigma_{\text{tot}}^{\bar{p}p}(s)$  and  $\sigma_{\text{tot}}^{pp}(s)$  at asymptotically high energies.

Now, we can apply the above procedure to study the behavior of the  $\rho$ -parameter as the collision energy grows. This parameter is defined as

$$\rho^{xp}(s) = \text{Re}F_{xp}(s)/\text{Im}F_{xp}(s), \quad (20)$$

which measures the rise of the absorptive part of the forward scattering amplitude (relative to the real part) as  $s$  grows.

If the condition (i) is used, then, from some  $s_a$ , the only possible result is  $\rho^{xp}(s_a < s) = 0$ , which does not contradict any theorem but has no predictive capability for non asymptotic energies. In contrast, adopting, for instance, assumption (iii), one obtains

$$\rho^{xp}(s) = c/[\pm a_1/\varepsilon + (2c/\pi) \ln \varepsilon], \quad (21)$$

where the sign  $+/-$  is for  $pp/\bar{p}p$ . For some sufficient high energy, the term  $a_1/\varepsilon$  can be disregarded, resulting the prediction that  $\rho^{pp}(s) = \rho^{\bar{p}p}(s)$  and  $\rho$ -parameter approaches to its asymptotic value ( $\rho_a$ )

$$\rho^{xp}(s)|_{s \rightarrow \infty} \rightarrow \rho_a^{xp}(s) \equiv (\pi/2) \ln^{-1} \varepsilon. \quad (22)$$

It is important to emphasize that (22) is independent of any external parameter, being the collision energy the only variable of interest. It seems to be reasonable since we expect the same parameters that drive  $\text{Im}F_{xp}(s)/s$  should also control  $\text{Re}F_{xp}(s)/s$ , at least for the high energy regime. Furthermore, the asymptotic result (22) agrees well with the "standard" picture of high energy elastic diffraction in which amplitude  $f_-(s)$  becomes negligible compared with the crossing-even one  $f_+(s)$  as  $s$  increases. The property of analyticity implies  $\rho \propto \ln^{-1} \varepsilon$  [22].

Results obtained for measured forward scattering parameters for  $\bar{p}p$  and  $pp$  within assumptions under consideration are summarized in Table II. It is interesting to point out that if we assume  $\rho(s)$  as given by assumptions (i), (ii), or (iii), then the use of DDR conduces to result similar to those obtained in [17]. In particular, assumptions (ii) and (iii) for  $\rho(s)$  result in  $\sigma_{\text{tot}}$  as given by Froissart–Martin bound, which means that it cannot be improved by the methods employed here.

TABLE II: Summary of the results for measured forward parameters assuming the asymptotic condition  $s \rightarrow \infty$ .

Assumption	$\sigma_{\text{tot}}^{\bar{p}p}(s)$	$\sigma_{\text{tot}}^{pp}(s)$	$\rho^{\bar{p}p}(s)$	$\rho^{pp}(s)$
(i)	$a_0/2 - a_1/\varepsilon$	$a_0/2 + a_1/\varepsilon$	0	0
(ii)	$\frac{3c_{\bar{p}} - c_p}{\pi} \ln \varepsilon - \frac{a_2}{\varepsilon}$	$\frac{3c_p - c_{\bar{p}}}{\pi} \ln \varepsilon + \frac{a_2}{\varepsilon}$	$\frac{c_{\bar{p}}}{[(3c_{\bar{p}} - c_p)/\pi] \ln \varepsilon - a_2/\varepsilon}$	$\frac{c_p}{[(3c_p - c_{\bar{p}})/\pi] \ln \varepsilon + a_2/\varepsilon}$
(iii)	$\frac{2c}{\pi} \ln \varepsilon - \frac{a_1}{\varepsilon}$	$\frac{2c}{\pi} \ln \varepsilon + \frac{a_1}{\varepsilon}$	$\frac{c}{(2c/\pi) \ln \varepsilon - a_1/\varepsilon}$	$\frac{c}{(2c/\pi) \ln \varepsilon + a_1/\varepsilon}$

In the framework of the present approach based on the crossing property, DDR (2), and optical theorem (3) both  $pp$  and  $\bar{p}p$  elastic collisions are characterized by similar energy dependencies for total cross section and  $\rho$ -parameter

at asymptotically high energies, namely,  $\forall x = p, \bar{p} : \sigma_{\text{tot}}^{xp}(s) \propto \ln \varepsilon$ ,  $\rho^{xp} \propto \ln^{-1} \varepsilon$  within more realistic assumptions (ii) and (iii), which are considered in this paragraph below.

It seems the dependence  $\sigma_{\text{tot}}^{xp}(s)$  for  $x = p, \bar{p}$  from Table II in the collision energy domain under consideration is functionally close to the increase of  $\sigma_{\text{tot}}^{pp}(s)$  deduced within Regge-eikonal approach [23]. But one can note  $\forall x = p, \bar{p} : \sigma_{\text{tot}}^{xp}(s)$  shows weaker increase with  $s$  than that within AQFT and semiclassical color glass condensate (CGC) approach which imply  $\sigma_{\text{tot}}(s)$  is functionally close to the Froissart–Martin limit (8) in the region, at least, of  $\mathcal{O}(100 \text{ TeV})$  energies [24]. The asymptotic behavior  $\forall x = p, \bar{p} : \rho^{xp}(s)|_{s \rightarrow \infty} \propto \ln^{-1} \varepsilon$  is qualitatively similar in functional sense to the corresponding AQFT  $\rho(s)$  dependencies for  $pp$  and  $\bar{p}p$  taking into account the values of fit parameters [25, 26].

### III. EXPERIMENTAL DATABASE AND FITTING PROCEDURE

The set of the global scattering parameters  $\mathcal{G}_1 \equiv \{\mathcal{G}_1^i\}_{i=1}^4 = \{\sigma_{\text{tot}}^{pp}, \sigma_{\text{tot}}^{\bar{p}p}, \rho^{pp}, \rho^{\bar{p}p}\}$  contains only observables which are independent on each other as well as directly measured in experiments. On the other hand, the set  $\mathcal{G}_2 \equiv \{\mathcal{G}_2^i\}_{i=1}^3 = \{\Delta_{\text{tot}}, \Sigma_{\text{tot}}, R_{\text{tot}}^{\bar{p}/p}\}$  is formed by the parameters, strictly speaking, depending on experimentally measurable quantities and, moreover, terms of  $\mathcal{G}_2$  are independent on each other as well as the terms of  $\mathcal{G}_1$ . In the present paper, the sets of scattering parameters and their combinations  $\mathcal{G}_j$ ,  $j = 1, 2$  are studied. Also the joined ensemble  $\mathcal{G} = \mathcal{G}_1 \cup \mathcal{G}_2$  is considered for completeness of information<sup>1</sup>.

The experimental database for  $\mathcal{G}_1$  contained the ensembles for  $\sigma_{\text{tot}}^{xp}$ ,  $\rho^{xp}$  from [16] is denoted as DB20 while the database taken into account the above samples and results from STAR for  $\sigma_{\text{tot}}^{pp}$  at  $\sqrt{s} = 0.20 \text{ TeV}$  [27] and from TOTEM for  $\rho^{pp}$  at  $\sqrt{s} = 13 \text{ TeV}$  [28] is referred as DB20+. The last paper leads to some uncertainty which result in two points of view for database creation. Two values  $\rho_1^{pp}|_{\sqrt{s}=13 \text{ TeV}} = 0.09 \pm 0.01$  and  $\rho_2^{pp}|_{\sqrt{s}=13 \text{ TeV}} = 0.10 \pm 0.01$  have been obtained in [28] for one quantity and collision energy without any preference for one value of  $\rho^{pp}$  on the another. On the other hand, the one result should be included in the corresponding data sample<sup>2</sup> because the  $\rho^{pp}$  was measured at the same experimental conditions (detector, kinematic parameters etc.). The weighted average [16] can be used as estimation for  $\rho^{pp}$  at  $\sqrt{s} = 13 \text{ TeV}$ :  $\langle \rho^{pp} \rangle|_{\sqrt{s}=13 \text{ TeV}} = 0.095 \pm 0.007$ . Therefore, two versions of the DB20+ are considered here, namely, the database with one value  $\langle \rho^{pp} \rangle|_{\sqrt{s}=13 \text{ TeV}}$  is the DB20<sub>1</sub>+ while the database contained both results  $(\rho_1^{pp}, \rho_2^{pp})$  at  $\sqrt{s} = 13 \text{ TeV}$  is denoted as DB20<sub>2</sub>+. Table III summarizes the main features of the databases of experimental results used in the present work for the set of the scattering parameters  $\mathcal{G}_1$ .

Within the present work main goals, the values for each term  $\{\mathcal{G}_2^i\}_{i=1}^3$  are calculated with the help of relations (5), (12) and measured values of  $\sigma_{\text{tot}}^{pp}$  and  $\sigma_{\text{tot}}^{\bar{p}p}$  for completeness of analysis. Below, these ensembles of calculated values are called as data samples for  $\mathcal{G}_2$  in similar with the set  $\mathcal{G}_1$  just in the sense that value of each term  $\{\mathcal{G}_2^i\}_{i=1}^3$  at certain  $s$  is only defined by experimental results for  $xp$  cross sections. The data sample for each term of  $\mathcal{G}_2$  is based on the corresponding subensembles for  $\sigma_{\text{tot}}^{pp}$  and  $\sigma_{\text{tot}}^{\bar{p}p}$  at identical or, at least, close energies<sup>3</sup>. As seen from Table III, the subensembles for  $\sigma_{\text{tot}}^{pp}$  and  $\sigma_{\text{tot}}^{\bar{p}p}$  from [16] are only used for calculation of the each term of  $\mathcal{G}_2$  and, consequently, there is one database for  $\mathcal{G}_2$  corresponded to the DB20 for  $\mathcal{G}_1$ . As expected from the definitions (5) and (12), the energy range covered by experiments is identical for all terms of  $\mathcal{G}_2$ . Detailed analysis shown that this range is limited to  $\sqrt{s} < 0.5 \text{ TeV}$  with wide gap between the highest ISR energy  $\sqrt{s} \approx 0.06 \text{ TeV}$  and the high energy boundary  $\sqrt{s} = (0.47 \pm 0.08) \text{ TeV}$  for the energy domain under discussion.

There is no prediction for the asymptotic energy  $\sqrt{s_a}$  from the first principles of QCD (for instance) as well as the search for the onset of the asymptotic energy domain remains a non-trivial task. Then, there is no consensus for the beginning of the so-called asymptotia. For example, the definition of the asymptotic regime may be done by using the first change of sign of the curvature parameter  $C$  in the impact parameter representation [32]. For the Chou–Yang model [33], for instance, the asymptotia begins at  $\sqrt{s_a} \approx 2 \text{ TeV}$ , where  $C$  changes its sign. However,

<sup>1</sup> In the paper total errors are used for experimental points unless otherwise specified. The total error is calculated as systematic error added in quadrature to statistical one.

<sup>2</sup> It should be stressed that such request is fully within the rules were applied for creation of experimental databases in various analyzes, for instance, for elastic slope [29] as well as in jet physics [30] and femtoscopy [31].

<sup>3</sup> The energy values for the measured  $\sigma_{\text{tot}}^{pp}$  and  $\sigma_{\text{tot}}^{\bar{p}p}$  are considered close if  $P_\Delta \equiv |P_1 - P_2| \leq 0.02 \text{ GeV}$  or  $P_1$  and  $P_2$  coincide within errors, where  $P_i$  is the laboratory momentum for the term  $\mathcal{G}_1^i$ ,  $i = 1, 2$ . One can note that the first condition for the closeness of  $P_1$  and  $P_2$  was previously used in [34]. The relative fraction of the pairs  $(\sigma_{\text{tot}}^{pp}, \sigma_{\text{tot}}^{\bar{p}p})$  with finite  $P_\Delta$  is 64.8% and almost all of such measurements are at  $\sqrt{s} < 3.63 \text{ GeV}$ . In these cases the average momentum  $\langle P \rangle$  is assigned for the initial energy for corresponding estimation of the each term  $\mathcal{G}_2^i$ ,  $i = 1 - 3$  and  $\langle P \rangle$  is calculated as simple average  $\langle P \rangle = 0.5(P_1 + P_2)$  with  $\Delta \langle P \rangle = 0.5|P_1 - P_2|$  if  $\exists i : \Delta P_i = 0$  or  $\langle P \rangle$  and its uncertainty is estimated with the help of the weighted average technique [16] on the contrary case.



recent studies show model-dependent estimations for  $s_a$ , and these values lies in a very wide energy range. From the experimental point of view, it seems the most optimistic estimation for  $\sqrt{s_a}$  is  $\mathcal{O}(100 \text{ TeV})$  in order of magnitude, and it was qualitatively obtained from the study of the functional behavior of  $\sigma_{\text{tot}}^{pp}(s)$  within AQFT and CGC approach at ultra-high energies [24]. This result agrees with the conclusion from the Regge–eikonal model for  $\sigma_{\text{tot}}^{pp}(s)$  and forward slope for  $pp$  interaction [23].

TABLE III: Databases for the set of global scattering parameters  $\mathcal{G}_1$ .

Database	Parameter from the set $\mathcal{G}_1$			
	$\sigma_{\text{tot}}^{pp}$	$\sigma_{\text{tot}}^{\bar{p}p}$	$\rho^{pp}$	$\rho^{\bar{p}p}$
DB20	[16]	[16]	[16]	[16]
DB20 <sub>1</sub> +	[16, 27]	—/—	[16] and $\langle \rho^{pp} \rangle _{\sqrt{s}=13 \text{ TeV}}$	—/—
DB20 <sub>2</sub> +	—/—	—/—	[16, 28]	—/—

Detailed analysis of the ratio of the elastic–to–total cross sections for  $pp$  and  $\bar{p}p$  collisions [34] as well as the approach of the partonic disks [35] allow only the indication  $\sqrt{s_a} \sim 5 - 10 \text{ PeV}$ . Consideration of some other signatures of the “truly asymptotic regime” within Regge–eikonal model [23] results in much more conservative estimation for  $s_a$ , in particular, the onset of the asymptotic regime can be expected in grand unified theory (GUT) energy domain in order of magnitude, i.e.  $\sqrt{s_a} \gtrsim 10^{12} - 10^{13} \text{ GeV}$ .

As seen, there are only 1 – 2 measurements for  $\sigma_{\text{tot}}^{pp}$  in ultra-high energy cosmic rays even for lowest estimation for  $\sqrt{s_a}$ . Therefore, a phenomenological approximation will be *a priori* at collision energies smaller than the possible onset of the asymptotic region. Consequently, the request for the validity of the Pomeranchuk theorem seems redundant for the energy range under fit, and one can consider the hypothesis (ii) as well as (iii) for the functional forms of the terms of  $\mathcal{G}$  within the fitting procedure. As previously [25, 26], the parameterizations shown in Table I and II for hypotheses (ii), (iii) will be applied for approximation of the energy dependence of different terms of  $\mathcal{G}$  only for  $s \geq s_{\text{min}}$ , where  $s_{\text{min}}$  is some empirical low boundary. During the analysis procedure, the  $s_{\text{min}}$  value will be decreased as much as possible in order to describe the wider energy domain with statistically reasonable fit quality.

#### IV. RESULTS OF SIMULTANEOUS FITS

The Section contains the detailed description of the results of simultaneous fits for the sets  $\mathcal{G}_i$ ,  $i = 1, 2$  and corresponding discussion.

##### A. Simultaneous Fits for the Set $\mathcal{G}_1$

The energy dependence of terms of  $\mathcal{G}_1$  is approximated at  $\sqrt{s_{\text{min}}} = 0.03, 0.04, 0.05, 0.06, 0.1, 0.5, 1, 5$  and  $10 \text{ TeV}$  by the corresponding formulas from Table II within hypothesis (ii) and (iii). At lowest  $s_{\text{min}}$  considered here the fit quality  $\chi^2/\text{n.d.f.} \approx 26$  with fast decrease at growth of the low boundary of fitted range for hypotheses (ii) and (iii). For both hypotheses considered the statistically reasonable fit qualities are only observed for  $\sqrt{s_{\text{min}}} \geq 0.06 \text{ TeV}$ . The present approach allows the reasonable description of  $\mathcal{G}_1$  within narrower energy ranges than that AQFT equations [25, 26] with shifting  $s_{\text{min}}$  towards larger values. In general, this result is expected because the asymptotic behavior of the total cross sections and  $\rho$ –parameter is studied here for  $pp$  and  $\bar{p}p$  collisions. Thus the discussion below is focused on the results for  $\sqrt{s_{\text{min}}} \geq 0.06 \text{ TeV}$ .

As seen from Table III, the data bases considered here differ from each other very slightly, more precisely, the maximum difference on 3 points is between DB20 and DB20<sub>2</sub>+. Furthermore, all of the experimental results which are addition with respect to the DB20 agree well with the general trends in the energy dependence of the corresponding observable. Therefore, in accordance with the hypothesis confirmed in [26] one can expect the negligible affect of the addition points on the values of fit parameters for various data bases at fixed  $s_{\text{min}}$ . Detailed analysis fully confirms the correctness of this suggestion for the results of simultaneous fits for  $\mathcal{G}_1$  with data bases DB20<sub>1</sub>+ and DB20<sub>2</sub>+ differ from each other only one point (Table III). The values of all fit parameters agrees within errors for DB20<sub>1</sub>+ and DB20<sub>2</sub>+ for each  $s_{\text{min}}$  and hypotheses (ii), (iii) considered here. Moreover, the identity is observed between numerical values of fit parameters and their uncertainties for DB20<sub>1</sub>+ and values for corresponding quantity for DB20<sub>2</sub>+ for the noticeable part of low boundaries  $s_{\text{min}}$ , especially within the hypothesis (iii). The approximation quality  $\chi^2/\text{n.d.f.}$  is

TABLE IV: Parameters for simultaneous fitting of  $\mathcal{G}_1(s)$  within various hypotheses at different stages of DB: DB20 (first line) and DB20<sub>1</sub>+ (second line).

$\sqrt{s_{\min}}$ , TeV	hypothesis (ii)				hypothesis (iii)		
	$c_p$ , mbarn	$c_{\bar{p}}$ , mbarn	$a_2$ , mbarn	$\chi^2/\text{n.d.f.}$	$c$ , mbarn	$a_1$ , mbarn	$\chi^2/\text{n.d.f.}$
0.06	$8.484 \pm 0.029$	$8.12 \pm 0.04$	$(-9.0 \pm 0.9) \times 10^3$	97.7/45	$8.342 \pm 0.024$	$(-1.9 \pm 0.6) \times 10^3$	170/46
	$8.468 \pm 0.029$	$8.12 \pm 0.04$	$(-8.5 \pm 0.9) \times 10^3$	108/47	$8.339 \pm 0.024$	$(-1.8 \pm 0.6) \times 10^3$	174/48
0.1	$8.35 \pm 0.04$	$7.91 \pm 0.06$	$(-1.0 \pm 0.4) \times 10^5$	39.6/34	$8.31 \pm 0.04$	$(2.8 \pm 1.5) \times 10^5$	124/35
	$8.35 \pm 0.04$	$7.91 \pm 0.06$	$(-1.2 \pm 0.5) \times 10^5$	43.7/36	$8.28 \pm 0.04$	$(2.2 \pm 0.9) \times 10^4$	134/37
0.5	$8.38 \pm 0.05$	$8.00 \pm 0.11$	$(3.1 \pm 1.4) \times 10^5$	37.1/30	$8.48 \pm 0.05$	$(2.04 \pm 0.25) \times 10^6$	62.3/31
	$8.39 \pm 0.05$	$8.01 \pm 0.11$	$(3.5 \pm 1.2) \times 10^5$	41.0/31	$8.48 \pm 0.05$	$(2.0 \pm 0.4) \times 10^6$	65.2/32
1	$8.28 \pm 0.17$	$7.6 \pm 0.6$	$(-1.9 \pm 0.5) \times 10^7$	33.0/23	$8.54 \pm 0.05$	$(1.8 \pm 0.4) \times 10^7$	34.9/24
	$8.4 \pm 0.3$	$8.0 \pm 1.1$	$(-2.4 \pm 0.8) \times 10^6$	37.3/24	$8.54 \pm 0.05$	$(1.9 \pm 0.4) \times 10^7$	37.9/25
5	$9.3 \pm 0.4$	$9.9 \pm 2.6$	$(-3.1 \pm 0.6) \times 10^8$	20.3/17	$9.03 \pm 0.21$	$(-3.1 \pm 0.8) \times 10^8$	20.5/18
	$9.35 \pm 0.15$	$10.0 \pm 1.9$	$(-3.1 \pm 0.6) \times 10^8$	21.4/18	$9.06 \pm 0.22$	$(-3.3 \pm 0.9) \times 10^8$	22.8/19
10	$9.4 \pm 1.7$	$10.1 \pm 2.7$	$(6.5 \pm 0.5) \times 10^7$	1.08/6	$9.1 \pm 1.0$	$(6.5 \pm 0.7) \times 10^7$	1.08/7
	$9.8 \pm 0.5$	$10.0 \pm 2.6$	$(-1.3 \pm 0.9) \times 10^9$	2.16/7	$9.9 \pm 0.6$	$(-1.7 \pm 0.8) \times 10^9$	2.26/8

very close for the simultaneous fits of DB20<sub>1</sub>+ and DB20<sub>2</sub>+ with subtle improvement for the last case at any fixed  $s_{\min}$ . All of these allows us to consider below the fit results obtained for DB20 and DB20<sub>1</sub>+

The numerical results of the simultaneous fits of  $\mathcal{G}_1$  in various energy ranges are shown in Tables IV for hypothesis (ii) and (iii). At fixed  $s_{\min}$  the first line is for DB20 as well as the second line shows results for DB20<sub>1</sub>+. Experimental data from DB20<sub>1</sub>+ for the terms  $\mathcal{G}_1^i$ ,  $i = 1 - 4$  together with fit curves are shown in Fig. 1 for  $\sqrt{s_{\min}} = 0.06$  TeV (solid lines) and at  $\sqrt{s_{\min}} = 1$  TeV (dashed lines). The thick curves are obtained within the hypothesis (ii) while the two remaining lines correspond to the hypothesis (iii).

The use of the multi-TeV values of  $\sqrt{s_{\min}}$  and the available experimental data within certain data base stipulates that the approximation procedure consequently transits from the simultaneous fit of the full set  $\mathcal{G}_1$  to the simultaneous fit of the  $pp$  observables  $\{\sigma_{\text{tot}}^{pp}, \rho^{pp}\}$  only at  $\sqrt{s_{\min}} = 5$  TeV and even to the individual fit of the  $\sigma_{\text{tot}}^{pp}$  at the highest  $\sqrt{s_{\min}} = 10$  TeV in the case of the DB20. In the last case, strictly speaking, hypothesis (ii) reduces to the hypothesis (iii) because of available experimental data allow the fix only the combination  $(3c_p - c_{\bar{p}})$ . There is no fitting function for which there would be, at least, one experimental point at  $\sqrt{s} \geq 10$  TeV and, at the same time, this function would contain parameter  $c_p$  or  $c_{\bar{p}}$  in the separate term. Moreover, one expects the smooth joining for the energy-dependent  $\bar{p}p$  global observables,  $\sigma_{\text{tot}}^{\bar{p}p}(s)$  and  $\rho^{\bar{p}p}(s)$ , in the experimentally measured range as well in the domain  $\sqrt{s} \geq 5$  (10) TeV described by the curve calculated from the fit results at  $\sqrt{s_{\min}} = 5$  (10) TeV. This expectation is established by the absence of the any signature for new physics beyond the Standard Model (SM) which could result in the sharp changing of the energy dependence of any global scattering parameter in  $pp/\bar{p}p$  collisions.

There are only few points for  $\rho^{xp}(s)$  in the TeV-energy domain and, moreover, the experimental values  $\rho^{xp} \sim 10^{-2}$  at  $\sqrt{s} > 1$  TeV; the consideration aforementioned in Sec. II implies the smooth behavior of the curves for  $\rho^{xp}(s)$  is dominated by the values of  $c_x / c$  parameters within hypothesis (ii) / (iii). Furthermore, changes in these curves are slow ( $\propto \ln^{-1} \varepsilon$ ) at sufficiently high  $s$ . All of these evidences result in relatively robust behavior of the curve for  $\rho^{\bar{p}p}(s)$  at  $\sqrt{s_{\min}} = 5, 10$  TeV as well as a reasonable agreement between experimental value of  $\rho^{\bar{p}p}(s)|_{\sqrt{s} \approx 2 \text{ TeV}}$  and analytic approximation in multi-TeV energy domain without any additional request for the smooth joining. Detailed analysis shows some influence of the request of the smooth joining for  $\sigma_{\text{tot}}^{\bar{p}p}(s)$  on the fit results within hypothesis (ii) for DB20<sub>1</sub>+ at  $\sqrt{s_{\min}} = 10$  TeV. For this case the numerical values of the fit parameters obtained taking into account the need of the smooth joining for  $\sigma_{\text{tot}}^{\bar{p}p}(s)$  are shown in Table IV while the results without additional request are following:  $c_p = (10.5 \pm 0.8)$  mbarn,  $c_{\bar{p}} = (13.2 \pm 2.8)$  mbarn,  $a_2 = (6.0 \pm 0.6) \times 10^7$  mbarn,  $\chi^2/\text{n.d.f.} = 1.08/7$ .

As seen the request of the smooth joining for  $\sigma_{\text{tot}}^{\bar{p}p}(s)$  influences on the value of  $a_2$  parameter and fit quality. If one releases the need under consideration, then one provides the agreement between values of  $a_2$  for various data bases within hypothesis (ii) at almost identical  $\chi^2/\text{n.d.f.}$ . Such exception results in the expected discrepancy between values of  $a_2$  and  $\chi^2/\text{n.d.f.}$  obtained by simultaneous fits within various hypotheses for data base DB20<sub>1</sub>+. One can note the change in the fit quality for the last two cases is noticeable but not at a first glance. It is important to point out that  $\chi^2/\text{n.d.f.}$  remains statistically acceptable for simultaneous fit of DB20<sub>1</sub>+ within hypothesis (ii) at highest  $s_{\min}$ , independently on additional request of the smooth joining for  $\sigma_{\text{tot}}^{\bar{p}p}(s)$ .

As observed from Table IV, the hypothesis (ii) allows the simultaneous approximation of all terms of  $\mathcal{G}_1$  with reasonable quality at  $\sqrt{s_{\min}} \geq 0.06$  TeV and with statistically acceptable one at  $\sqrt{s_{\min}} \geq 0.1$  TeV for any data bases considered. The following relation  $c_p > c_{\bar{p}}$  is valid for the simultaneous fit versions within hypothesis (ii) up to



TABLE V: Parameters for simultaneous fitting of  $\mathcal{G}_1(s)$  within various hypotheses at different stages of the accelerator subsample of DB: DB<sub>ac</sub>20 (first line) and DB<sub>ac</sub>20<sub>1</sub>+ (second line).

$\sqrt{s_{\min}}$ , TeV	hypothesis (ii)				hypothesis (iii)		
	$c_p$ , mbarn	$c_{\bar{p}}$ , mbarn	$a_2$ , mbarn	$\chi^2/\text{n.d.f.}$	$c$ , mbarn	$a_1$ , mbarn	$\chi^2/\text{n.d.f.}$
0.06	$8.49 \pm 0.03$	$8.12 \pm 0.04$	$(-9.1 \pm 0.9) \times 10^3$	92.1/31	$8.343 \pm 0.024$	$(-1.9 \pm 0.6) \times 10^3$	165/32
	$8.471 \pm 0.029$	$8.12 \pm 0.04$	$(-8.6 \pm 0.9) \times 10^3$	103/33	$8.339 \pm 0.024$	$(-1.8 \pm 0.6) \times 10^3$	169/34
0.1		—				—	
	$8.35 \pm 0.04$	$7.91 \pm 0.06$	$(-1.2 \pm 0.6) \times 10^5$	40.2/23	$8.28 \pm 0.04$	$(4.4 \pm 0.8) \times 10^4$	129/24
0.5	$8.38 \pm 0.05$	$8.00 \pm 0.11$	$(3.1 \pm 1.4) \times 10^5$	35.0/21	$8.48 \pm 0.05$	$(2.03 \pm 0.25) \times 10^6$	59.9/22
	$8.38 \pm 0.05$	$8.01 \pm 0.11$	$(3.5 \pm 0.9) \times 10^5$	39.0/22	$8.48 \pm 0.05$	$(2.03 \pm 0.25) \times 10^6$	62.9/23
1	$8.29 \pm 0.16$	$7.7 \pm 0.5$	$(-1.7 \pm 0.8) \times 10^7$	31.0/14	$8.54 \pm 0.05$	$(1.9 \pm 0.4) \times 10^7$	32.8/15
	$8.39 \pm 0.05$	$8.02 \pm 0.11$	$(-2.4 \pm 0.5) \times 10^6$	35.3/15	$8.54 \pm 0.05$	$(1.9 \pm 0.4) \times 10^7$	35.8/16
5	$9.34 \pm 0.16$	$10.0 \pm 2.7$	$(-2.9 \pm 0.7) \times 10^8$	19.0/8	$9.01 \pm 0.23$	$(-3.0 \pm 0.9) \times 10^8$	19.2/9
	$9.33 \pm 0.16$	$10.0 \pm 1.9$	$(-2.9 \pm 0.8) \times 10^8$	20.1/9	$9.04 \pm 0.23$	$(-3.2 \pm 0.7) \times 10^8$	21.5/10
10		—				—	
		—			$10.5 \pm 0.7$	$(-2.7 \pm 0.7) \times 10^9$	0.05/1

$\sqrt{s_{\min}} = 0.5$  TeV. On the other hand, the values of  $c_p$  and  $c_{\bar{p}}$  coincide within errors for approximations at  $\sqrt{s_{\min}} \geq 1$  TeV. These statements are valid for both data bases DB20 and DB20<sub>1</sub>+. It is important to note that for the hypothesis (iii), in contrast with (ii), a reasonable values of  $\chi^2/\text{n.d.f.}$  can be obtained only at  $\sqrt{s_{\min}} \geq 0.5$  TeV and statistically acceptable  $\chi^2/\text{n.d.f.}$  – only at  $\sqrt{s_{\min}} \geq 1$  TeV. This feature is in full agreement with Table IV: as consequence of the considered relations between  $c_p$  and  $c_{\bar{p}}$  at various  $s_{\min}$ , it can be expected that reducing the parameters  $c_p$ ,  $c_{\bar{p}}$  to  $c$  would be possible starting, at least, at similar collision energies<sup>4</sup>. Thus, hypothesis (iii) reasonably describes the experimental data for  $\mathcal{G}_1$  at substantially higher  $s$  than the hypothesis (ii) due to "extremely" asymptotic nature of the corresponding relations in Table II. The hypotheses (ii) and (iii) qualitatively describe the energy-dependent behavior of  $\sigma_{\text{tot}}^{xp}$  at  $\sqrt{s_{\min}} = 0.06$  TeV already (Fig. 1a, b). However, they give overestimates for the  $\rho^{xp}$  at  $\sqrt{s} < 0.1$  TeV (Fig. 1c, d) which allows the qualitative assumption that discrepancy between experimental values of  $\rho^{xp}$  and smooth curves within hypotheses (ii) and (iii) at  $\sqrt{s} < 0.1$  TeV is the main reason for the large values of  $\chi^2/\text{n.d.f.}$  for simultaneous fits at small values of low boundary of the fitted range considered here ( $\sqrt{s_{\min}} = 0.03, 0.04$  and  $0.05$  TeV).

Comparative analysis of the fit parameters obtained for data bases DB20 and DB20<sub>1</sub>+ and shown in Table IV results in the following conclusions: (a) close values of  $\chi^2/\text{n.d.f.}$  are for both data bases at any fixed  $s_{\min}$ ; (b) values of  $c_p$ ,  $c_{\bar{p}}$  within hypothesis (ii) agrees within errors for various data bases at corresponded  $s_{\min}$  as well as values of  $c$  in the case of the hypothesis (iii); (c) mostly the last statement is also valid for parameter  $a_2/a_1$  for the hypothesis (ii) / (iii).

In general, the versions (ii) and (iii) of the asymptotic model suggested within the present work describe the experimental data for the set  $\mathcal{G}_1$  at higher energies than AQFT [25, 26], especially the hypothesis (iii). The comparison between the asymptotic model and AQFT is possible only at  $\sqrt{s_{\min}} = 0.06$  TeV, and fit quality is noticeably worse in the first case than that for AQFT. Such a relationship between the phenomenological models is expected, since the approach considered here is *a priori* asymptotic, i.e. as reasonably expect the model based on the suggestions allowed for the asymptotic energy domain will describe of the experimental data well at higher, strictly speaking, asymptotically high energies.

The ensemble of experimental results that includes only accelerator data is also considered for each data base DB20, DB20<sub>1</sub>+ and DB20<sub>2</sub>+. These ensembles are denoted as DB<sub>ac</sub>20, DB<sub>ac</sub>20<sub>1</sub>+ and DB<sub>ac</sub>20<sub>2</sub>+. The energy dependence of terms of  $\mathcal{G}_1$  is approximated at  $\sqrt{s_{\min}} = 0.03, 0.04, 0.05, 0.06, 0.1, 0.5, 1, 5$  and  $10$  TeV by the corresponding formulas from Table II within hypothesis (ii) and (iii) for each ensemble DB<sub>ac</sub>20, DB<sub>ac</sub>20<sub>1</sub>+ and DB<sub>ac</sub>20<sub>2</sub>+ as well as for the full data bases above. The statement made for DB20, DB20<sub>1</sub>+ and DB20<sub>2</sub>+ with regards of fit qualities is valid for this case. Therefore the discussion below for samples DB<sub>ac</sub>20, DB<sub>ac</sub>20<sub>1</sub>+ and DB<sub>ac</sub>20<sub>2</sub>+ is focused on the results for  $\sqrt{s_{\min}} \geq 0.06$  TeV.

<sup>4</sup> Strictly speaking, the possible reduction of the number of fit parameters does not mean the transition from the hypothesis (ii) to the (iii) one because the corresponding fit parameters obtained within these hypotheses disagree for DB20 at  $\sqrt{s_{\min}} = 1$  TeV and similar statement is for  $a_1$  and  $a_2$  parameters in the case of DB20<sub>1</sub>+.

The values of all fit parameters agree quite well within errors for  $\text{DB}_{\text{ac}}20_1+$  and  $\text{DB}_{\text{ac}}20_2+$  for each  $s_{\text{min}}$  and hypotheses (ii), (iii) considered here. The approximation quality  $\chi^2/\text{n.d.f.}$  is very close for the simultaneous fits of accelerator data ensembles  $\text{DB}_{\text{ac}}20_1+$  and  $\text{DB}_{\text{ac}}20_2+$  with subtle improvement for the last case at any fixed  $s_{\text{min}}$ . These statements are valid with exception of the highest  $\sqrt{s_{\text{min}}} = 10$  TeV analyzed below more detailed. As well as for the full data bases all of these allows us to consider below the fit results for  $\text{DB}_{\text{ac}}20$  and  $\text{DB}_{\text{ac}}20_1+$ .

The numerical results of the simultaneous fits of  $\mathcal{G}_1$  in various energy ranges are shown in Tables V for hypothesis (ii) and (iii) taking into account the accelerator data only. At fixed  $s_{\text{min}}$  the first line is for  $\text{DB}_{\text{ac}}20$  and second line shows results for  $\text{DB}_{\text{ac}}20_1+$ . Experimental data from  $\text{DB}_{\text{ac}}20_1+$  for the terms  $\mathcal{G}_1^i$ ,  $i = 1 - 4$  together with fit curves are shown in Fig. 2 for  $\sqrt{s_{\text{min}}} = 0.06$  TeV (solid lines) and at  $\sqrt{s_{\text{min}}} = 1$  TeV (dashed lines). The thick curves are obtained within the hypothesis (ii) and the two other lines correspond to the hypothesis (iii). The energy domain  $\sqrt{s} \geq 0.06$  TeV is considered in Fig. 2 in difference with Fig. 1 in order to show fit curves clearer for different  $s_{\text{min}}$  and hypotheses.

Numerical values for the fit parameters agree within errors for Tables IV and V at fixed  $s_{\text{min}}$  and hypothesis. Therefore, most of conclusions made above for the full data bases  $\text{DB}20$ ,  $\text{DB}20_1+$  and  $\text{DB}20_2+$  are valid for the corresponded ensembles of the accelerator experimental results with the following features and interpretations. There are agreement, within errors, between the numerical values of the corresponded fit parameters for ensembles  $\text{DB}_{\text{ac}}20$  and  $\text{DB}_{\text{ac}}20_1+$  for certain hypothesis and fixed  $s_{\text{min}}$ . Furthermore, values are identical for free parameters at  $\sqrt{s_{\text{min}}} = 0.5$  and 1 TeV within hypothesis (iii). As consequence, the fit curves for various hypotheses are close for each other at any fixed  $s_{\text{min}}$  considered in Fig. 2 for each observable from the set  $\mathcal{G}_1$ .

Table V shows that there is noticeable decreasing of the relative uncertainties for  $c$  at  $\sqrt{s_{\text{min}}} = 1$  TeV, for  $c_{\bar{p}}$  at  $\sqrt{s_{\text{min}}} \geq 1$  TeV, for  $a_2$  at  $\sqrt{s_{\text{min}}} = 0.5$  and 1 TeV at transition from the ensemble  $\text{DB}_{\text{ac}}20$  to  $\text{DB}_{\text{ac}}20_1+$  one for hypothesis (ii). The similar effect is absent for pairs of any other ensembles at certain hypothesis. The data sets for approximation are identical for  $\sqrt{s_{\text{min}}} = 0.1$  and 0.5 TeV in the case of the sample  $\text{DB}_{\text{ac}}20$  wherefore the fit results are only shown in the last case in Table V. The fits are impossible at highest  $\sqrt{s_{\text{min}}} = 10$  TeV due to lack of the required number of data points with exception of the cases of  $\text{DB}_{\text{ac}}20_1+$  for hypothesis (iii), shown in Table V and ensemble  $\text{DB}_{\text{ac}}20_2+$  for both hypotheses under study. In the last case the following results are obtained with help of the simultaneous fit at highest  $\sqrt{s_{\text{min}}} = 10$  TeV:  $c_p = (10.00 \pm 0.13)$  mbarn,  $c_{\bar{p}} = (10.0 \pm 1.7)$  mbarn,  $a_2 = (-1.8 \pm 1.0) \times 10^9$  mbarn,  $\chi^2/\text{n.d.f.} = 0.88/1$  for the hypothesis (ii) and  $c = (10.5 \pm 0.7)$  mbarn,  $a_1 = (-2.7 \pm 0.7) \times 10^9$  mbarn,  $\chi^2/\text{n.d.f.} = 0.55/2$  – hypothesis (iii).

These data confirm all conclusions made above regarding of the agreement between fitting results for  $\text{DB}_{\text{ac}}20_1+$  (Table V) and  $\text{DB}_{\text{ac}}20_2+$  in the case of the hypothesis (iii) and between the full data base  $\text{DB}20_1+$ ,  $\text{DB}20_2+$  and corresponding ensembles of accelerator experimental results for hypothesis (ii) at  $\sqrt{s_{\text{min}}} = 10$  TeV taking into account the closeness of the results of approximation established above for  $\text{DB}20_1+$  and  $\text{DB}20_2+$ .

One can note that the fitting results are obtained with the request for the smooth joining of the  $\sigma_{\text{tot}}^{\bar{p}p}(s)$  and  $\rho^{\bar{p}p}(s)$  in experimentally measured range and in the domain  $\sqrt{s} \geq 5$  (10) TeV within hypothesis (ii) at  $\sqrt{s_{\text{min}}} = 5$  TeV for the ensembles  $\text{DB}_{\text{ac}}20$ ,  $\text{DB}_{\text{ac}}20_1+$  (Table V) and at  $\sqrt{s_{\text{min}}} = 5$  and 10 TeV for  $\text{DB}_{\text{ac}}20_2+$ . As seen from Tables IV and V, the exception of the cosmic ray (CR) measurements result in the deterioration in the quality of the approximation for the ensembles  $\text{DB}_{\text{ac}}20$  and  $\text{DB}_{\text{ac}}20_1+$  regarding of the corresponded full data bases<sup>5</sup>. Only statistically reasonable values of  $\chi^2/\text{n.d.f.}$  are obtained for ensembles of accelerator results for any  $\sqrt{s_{\text{min}}} \geq 0.06$  TeV in difference with the full data bases. Consequently, hypotheses (ii) and (iii) allow the qualitative description of energy dependence of  $\mathcal{G}_1$  only. Fig. 2 demonstrates the qualitative agreement of the curves from simultaneous fits of the terms of  $\mathcal{G}_1$  with data points at any considered  $s_{\text{min}}$ . The main features of the behavior of these fit curves with respect to the experimental results are similar to those observed in Fig. 1 at corresponded  $s_{\text{min}}$ .

In general, one can conclude the exclusion of the CR data from the fitted samples results in to significant narrowing of the experimentally available energy domain due to decreasing of the maximal energy boundary from  $\sqrt{s} = 95_{-8}^{+5}$  TeV [36] down to the  $\sqrt{s} = 13$  TeV at the LHC, and noticeable deterioration of approximation quality in the most cases. Therefore, the full data bases from Table III are considered below as well as corresponding fitting results from Table IV unless otherwise stated.

One can note that the curves obtained within the hypothesis (iii) at  $\sqrt{s_{\text{min}}} = 1$  TeV show some peculiar behavior close to the lower boundary of the fitted range (Figs. 1 and 2). This behavior is dominated by the standard-fit procedure, namely, by the request to obtain a better fit quality and the absence of experimental points close to  $\sqrt{s_{\text{min}}} = 1$  TeV. Therefore, this peculiar behavior is an artificial effect due to the data analysis procedure. Furthermore, the fit at  $s \geq s_{\text{min}}$ , obviously, does not take into account data points at lower  $s$ , consequently, the behavior under

<sup>5</sup> The case of the  $\sqrt{s_{\text{min}}} = 10$  TeV is special one because there only are 1 or 2 n.d.f. if any for  $\text{DB}_{\text{ac}}20_1+$  and  $\text{DB}_{\text{ac}}20_2+$  respectively. Thus the results obtained for so small n.d.f. can not be considered as representative.

consideration does not contradict any physical results and it has no physical meaning. The hypothesis (ii) is less sensitive to the absence / presence of the data points closer to  $\sqrt{s} \approx 1$  TeV than hypothesis (iii). Accordingly, the curves obtained within the hypothesis (ii) at  $\sqrt{s_{\min}} = 1$  TeV shows a smooth behavior without any features at low energy edge (thick dashed lines in Figs. 1 and 2) whereas the curves obtained using hypothesis (iii) at  $\sqrt{s_{\min}} = 1$  TeV shows the peculiar behavior at low energy edge (thin dashed lines in Figs. 1 and 2) due to the aforementioned reasons.

In summary, for this subsection, simultaneous fit results obtained for the full data bases DB20, DB20<sub>1</sub>+ and DB20<sub>2</sub>+ as well as for the corresponding ensembles of accelerator data DB<sub>ac</sub>20, DB<sub>ac</sub>20<sub>1</sub>+ and DB<sub>ac</sub>20<sub>2</sub>+ indicates, in general, the robustness of the fit results for each hypothesis under consideration for fixed  $s_{\min}$ , and on the value of the lower boundary of fitted range for  $\sqrt{s_{\min}} \geq 0.06$  TeV within certain hypotheses (Tables IV and V). As a consequence, the corresponding curves are closer to each other in Figs. 1 and 2.

## B. Simultaneous Fits for the Set $\mathcal{G}_2$

Fig. 3 shows the energy dependence for  $\mathcal{G}_2$ , namely  $\Delta_{\text{tot}}$  (a),  $\Sigma_{\text{tot}}$  (b) and  $R_{\text{tot}}^{\bar{p}/p}$  (c), with the values of points multiplied on 0.1 in Fig. 3b for  $\Sigma_{\text{tot}}(s)$  in order to use the one scale for the  $Y$ -axis for the terms  $\mathcal{G}_2^1$  and  $\mathcal{G}_2^2$ . It can be seen from the plots for terms of  $\mathcal{G}_2$  that values of any term  $\mathcal{G}_2^i$ ,  $i = 1 - 3$  decrease at  $\sqrt{s} \lesssim 10$  GeV, especially fast at  $\sqrt{s} < 3$  GeV. For higher energies the slowdown is observed in the decrease for  $\Delta_{\text{tot}}$  (Fig. 3a) and  $R_{\text{tot}}^{\bar{p}/p}$  (Fig. 3c), especially noticeable in the last case; a broad minimum occurs for  $\Sigma_{\text{tot}}$  (Fig. 3b), followed by a moderate increase at  $\sqrt{s} \gtrsim 20$  GeV.

One can note that the values of  $\Delta_{\text{tot}}$  and  $R_{\text{tot}}^{\bar{p}/p}$  at highest available energy are larger than the previous measurements, especially in the first case. However, since this is the only point for each parameter  $\Delta_{\text{tot}}$  and  $R_{\text{tot}}^{\bar{p}/p}$ , this increasing can be only considered as an indication on a possible transition to growth at  $\sqrt{s} > 62$  GeV, i.e. at energies larger than the maximum energy of ISR, in the corresponding energy dependence. Except for three points with large errors  $\Delta_{\text{tot}} \geq 1 - 2$  mb;  $R_{\text{tot}}^{\bar{p}/p} > 1$  although it approaches to the asymptotic value (12) from above with an accuracy level better than 2% at ISR energies. However, indications on the change in the behavior of the  $\Delta_{\text{tot}}(s)$  and  $R_{\text{tot}}^{\bar{p}/p}(s)$  at higher energies, the absence of an exact reaching of the asymptotic levels and continuation of this trend at any higher energies, as well as other numerous studies, make it possible to exclude the reach of the asymptotic regime at ISR energies.

The energy dependence of terms of  $\mathcal{G}_2$  is approximated at  $\sqrt{s_{\min}} = 3, 5, 10, 15, 20, 25, 30, 40, 50, 60$  and 100 GeV by the corresponding formulas from Table I within hypothesis (ii) and (iii). It should be noted that the fitted samples and, as consequence, numerical values of the fit parameters are identical for the pairs (25, 30) GeV and (40, 50) GeV of the values of  $\sqrt{s_{\min}}$ . Due to detailed analysis, one obtains that analytic formulas from Table I describe quite poor the energy dependence of terms of  $\mathcal{G}_2$  at most of values of  $\sqrt{s_{\min}}$  for hypotheses (ii) and (iii). The qualitative analysis indicates that large values of  $\chi^2/\text{n.d.f.}$  are mostly dominated by the large discrepancy between fit curves and data points for  $\Sigma_{\text{tot}}(s)$ . For both hypotheses, the value of  $\chi^2/\text{n.d.f.}$  decreases fast at growth of the low boundary of fitted range and the qualitative agreement is achieved for fitted curves and data points at  $\sqrt{s_{\min}} \geq 25$  GeV. Reasonable fit qualities are only observed for  $\sqrt{s_{\min}} \geq 40$  GeV. As well as for  $\mathcal{G}_1$  such relation between fits and data can be considered as expected because the formulas from Table I are asymptotic, especially for the hypothesis (iii). On the other hand, experimental data for  $\mathcal{G}_2$  are only available for  $\sqrt{s} < 0.5$  TeV. This energy range is significantly narrower even than that for  $\mathcal{G}_1$  and such collision energies are far from any estimation for the onset of the asymptotic region. Thus the discussion below is focused on the results for  $\sqrt{s_{\min}} \geq 0.03$  TeV with taking into account the identity of data samples for  $\sqrt{s_{\min}} = 25$  and 30 GeV noted above.

Fig. 3 shows the results of the simultaneous fits of corresponding data samples by using (5) and (12) as solid (dashed) lines for  $\sqrt{s_{\min}} = 0.03$  (0.06) TeV. The thick lines show the fit curves for the hypothesis (ii) and the two other lines correspond to the hypothesis (iii). The curves are also multiplied on 0.1 in Fig. 3b in order to correspond to the scaled data points for  $\Sigma_{\text{tot}}(s)$ . The numerical values of fit parameters are shown in Table VI for some  $\sqrt{s_{\min}} \geq 0.03$  TeV. For the hypothesis (ii) the fit is impossible at highest  $\sqrt{s_{\min}} = 0.10$  TeV considered in this section due to lack of the required number of data points.

As seen in Table VI, the values of  $c_p$  and  $c_{\bar{p}}$  agree with each other within 1.25 standard deviation or better at  $\sqrt{s_{\min}} \geq 0.03$  TeV, i.e. for the fits described data points, at least, qualitatively. The values of  $c_p$  and  $c_{\bar{p}}$  decrease continuously with growth of  $\sqrt{s_{\min}}$ , with exception of  $c_{\bar{p}}$  at highest available  $\sqrt{s_{\min}} = 0.06$  TeV, that coincides with the value of the parameter at  $\sqrt{s_{\min}} = 0.05$  TeV. The similar situation is observed in Table VI for  $c$  parameter in the case of the hypothesis (iii).

It is not possible to identify any trend in the behavior of  $a_1$  depending on  $s_{\min}$  due to the small number of obtained values of the free parameter for hypothesis (ii). For other hypothesis studied here,  $a_1$  is almost constant within

TABLE VI: Parameters for simultaneous fitting of  $\mathcal{G}_2(s)$  within various hypotheses.

$\sqrt{s_{\min}}$ , TeV	hypothesis (ii)				hypothesis (iii)		
	$c_p$ , mbarn	$c_{\bar{p}}$ , mbarn	$a_2$ , mbarn	$\chi^2/\text{n.d.f.}$	$c$ , mbarn	$a_1$ , mbarn	$\chi^2/\text{n.d.f.}$
0.03	$8.72 \pm 0.03$	$8.78 \pm 0.03$	$-900 \pm 200$	398/12	$8.750 \pm 0.024$	$(-1.27 \pm 0.12) \times 10^3$	404/13
0.05	$8.49 \pm 0.06$	$8.46 \pm 0.06$	$(-2.7 \pm 0.5) \times 10^3$	31.3/9	$8.475 \pm 0.028$	$(-2.1 \pm 0.4) \times 10^3$	31.4/10
0.06	$8.34 \pm 0.04$	$8.44 \pm 0.04$	$-0.15 \pm 0.07$	7.64/6	$8.39 \pm 0.03$	$(-1.9 \pm 0.5) \times 10^3$	8.17/7
0.10	—	—	—	—	$7.7 \pm 0.7$	$(-4.5 \pm 0.6) \times 10^4$	2.17/1

uncertainties with exception the value at highest available  $\sqrt{s_{\min}} = 0.10$  TeV. Detailed analysis shows that the fit results are not stable enough at highest available  $s_{\min}$  for both hypotheses. The corresponding approximated curves for  $\Delta_{\text{tot}}(s)$  and  $R_{\text{tot}}^{\bar{p}/p}(s)$  can show very sharp behavior with clear contradictions to both the data points and the general trends in the energy dependence of  $\Delta_{\text{tot}}$  and  $R_{\text{tot}}^{\bar{p}/p}$ . This situation is similar to that observed for the set  $\mathcal{G}_1$  and discussed above in subsec. IV A. Therefore, by analogy with the study of  $\mathcal{G}_1$ , Table VI shows the values of fitted parameters obtained accounting for the additional request of smooth behavior of curves and their qualitative agreement with nearest data points at smaller collision energies for  $\sqrt{s_{\min}} = 0.06 / 0.10$  TeV for hypothesis (ii) / (iii).

Fig. 3a shows the curve for  $\Delta_{\text{tot}}$  obtained from the simultaneous fit at  $\sqrt{s_{\min}} = 0.03$  TeV within hypothesis (ii) corresponds at qualitative level to the main features of the energy dependence of data points, namely, the decrease of  $\Delta_{\text{tot}}(s)$  at  $\sqrt{s} \lesssim 60$  GeV and the possible increase of this parameter at higher collision energies, despite of large  $\chi^2/\text{n.d.f.}$  On the other hand the formulas in Table I for  $\Delta_{\text{tot}}(s)$  and  $\Sigma_{\text{tot}}(s)$  within hypothesis (iii) show only smooth decrease ( $\propto \varepsilon^{-1}$ ) or increase ( $\propto \ln \varepsilon$ ) respectively without any dependence on fitted energy range and, as consequence, it is difficult to describe the change of behavior of the  $s$ -dependence of terms of the set  $\mathcal{G}_2$  within hypothesis (iii) as seen most clear in Fig. 3a for  $\Delta_{\text{tot}}(s)$ . The fitted curves for  $\Sigma_{\text{tot}}$  (Fig. 3b) and  $R_{\text{tot}}^{\bar{p}/p}$  (Fig. 3c) are (very) close to each other at  $\sqrt{s_{\min}} = 0.03$  and  $0.06$  TeV within certain hypothesis and for various hypotheses at fixed  $s_{\min}$ .

Summarizing, the detailed analysis of the energy dependence of terms of the set  $\mathcal{G}_2$  excludes the possibility of an asymptotic regime at ISR energies, and that agrees with numerous studies. The analytic functions deduced within the hypotheses (ii) and (iii) for the energy dependence of terms  $\{\mathcal{G}_2^i\}_{i=1}^3$  describe the experimental data at qualitative level for  $\sqrt{s_{\min}} \geq 40$  GeV only. The curves for  $\Delta_{\text{tot}}(s)$  obtained with the help of the simultaneous fits for  $\mathcal{G}_2$  are sensitive for both hypotheses and the value of  $s_{\min}$  (Fig. 3a). In contrast, simultaneous fit results lead to the curves for  $\Sigma_{\text{tot}}$  (Fig. 3b) and  $R_{\text{tot}}^{\bar{p}/p}$  (Fig. 3c) which are almost independent on the hypothesis type for a fixed  $s_{\min}$  and the value of  $s_{\min}$  for certain hypotheses.

### C. Consideration for the Joined Ensemble $\mathcal{G}$

The simultaneous fit of the terms of  $\mathcal{G}$  is not possible because, as emphasized in Sec. III, the databases for the terms of  $\mathcal{G}_2$  are calculated from the experimental values of some parameters of  $\mathcal{G}_1$ , namely, from the measurements<sup>6</sup> of  $\sigma_{\text{tot}}^{xp}$ ,  $x = p, \bar{p}$ . On the other hand, all terms of the joined ensemble  $\mathcal{G}$  are defined by the one set of the free parameters within certain hypothesis (ii) or (iii) suggested within the present work. Therefore, the energy dependence for the terms of one set from  $\mathcal{G}_1$ ,  $\mathcal{G}_2$  can be calculated with help of the values of free parameters obtained from the simultaneous fit of the terms of the another set called below as "adjoint set", i.e. the curves for smooth energy dependence of the terms of  $\mathcal{G}_1$  at fixed  $s_{\min}$  can be calculated with the free parameter values obtained for  $\mathcal{G}_2$  by the simultaneous fit at the same  $s_{\min}$ , and vice versa.

Fig. 4 shows the energy dependence for the terms of  $\mathcal{G}$  derived within hypothesis (ii) at  $\sqrt{s_{\min}} = 0.06$  TeV. Database DB20<sub>1+</sub> is used for the terms of  $\mathcal{G}_1$ . The thick curves are from the simultaneous fits for the terms of  $\mathcal{G}_i$ ,  $i = 1, 2$  whereas the thin lines correspond to the results of the calculations for some term from  $\mathcal{G}_i$ ,  $i = 1, 2$  with help of the values of free parameters obtained for the adjointed set  $\mathcal{G}_j$ ,  $j \neq i$  by simultaneous fit and shown in Tables IV and VI for  $\sqrt{s_{\min}} = 0.06$  TeV. Lines corresponded to the fit results and calculations are close to each other for  $\mathcal{G}_1$  (Figs. 4a–d), but the situation is different for most terms of  $\mathcal{G}_2$ . There is dramatic discrepancy between fitted and calculated curves

<sup>6</sup> One can note this situation principally differs from the situation for databases for  $\sigma_{\text{tot}}$ , elastic ( $\sigma_{\text{el}}$ ) and inelastic ( $\sigma_{\text{inel}}$ ) cross sections which are related by the optical theorem. There are number of experiments measured  $\sigma_{\text{inel}}$  directly, for instance, [37]. Therefore the databases for the set  $\{\sigma_{\text{tot}}, \sigma_{\text{el}}, \sigma_{\text{inel}}\}$  can be considered as, at least, particularly independent.



for  $\Delta_{\text{tot}}(s)$  in Fig. 4e whereas the parameter  $\Sigma_{\text{tot}}$  is not sensitive to the technique of the creation of smooth curve at all (Fig. 4f); two curves show the similar behavior in functional sense at  $\sqrt{s} \geq 0.2$  TeV, but there is quantitative difference between them for  $R_{\text{tot}}^{\bar{p}/p}(s)$  in Fig. 4g.

These features for the terms of  $\mathcal{G}_2$  are driven by the unstable behavior of the fit results for  $\mathcal{G}_2$  at  $\sqrt{s_{\text{min}}} = 0.06$  TeV within hypothesis (ii) as well as the special request added for the simultaneous fit for  $\mathcal{G}_2$  described in the subsec. IV B. This suggestion is confirmed in Fig. 5, that shows the energy dependence for the terms of  $\mathcal{G}$  derived within hypothesis (iii) at  $\sqrt{s_{\text{min}}} = 0.06$  TeV. In this case the fit results for  $\mathcal{G}_2$  are stable and additional request are not used for the fit procedure at all. Fig. 5 shows the full identity of the fitted and calculated curves for each term of the joined ensemble  $\mathcal{G}$  due to agreement of the values of free parameters within errors in Table IV and VI for hypothesis (iii) at  $\sqrt{s_{\text{min}}} = 0.06$  TeV.

It should be noted from Figs. 4 and 5 that, in general, one can obtain the smooth energy dependence for the terms of  $\mathcal{G}_1$  in multi-TeV range with help of the fit results for  $\mathcal{G}_2$  at much smaller collision energies. Moreover, the calculated curves for  $\mathcal{G}_1$  agree with both the experimental points and the corresponding fitted curves, at least, reasonably. Thus, the trends in the  $s$ -dependence of the terms of  $\mathcal{G}_2$  observed at  $\sqrt{s} \lesssim 0.5$  TeV and driven by the behavior of the  $\sigma_{\text{tot}}^{xp}(s)$ ,  $x = p, \bar{p}$  allow us to obtain the correct energy dependence for the terms of  $\mathcal{G}_1$  in much wider energy domain up to the highest  $s$  available in experiments.

Summarizing this subsection: the energy dependence for each term of the joined set  $\mathcal{G}$  can be calculated using the free parameter values obtained for any separate set  $\mathcal{G}_i$ ,  $i = 1, 2$  by the simultaneous fit within the validity of the additional request of stability for the results of that simultaneous fit for  $\mathcal{G}_i$ ,  $i = 1, 2$ .

## V. DISCUSSION AND PROJECTIONS FOR GLOBAL SCATTERING PARAMETERS

First of all, the results shown in Table IV allow the qualitative estimation of the onset of asymptotic energy domain  $s_a$ . As seen along the text,  $c_p, c_{\bar{p}}$  agree with  $c$  within errors as well as  $a_2$  with  $a_1$  for simultaneous fits within hypotheses (ii) and (iii) at  $\sqrt{s_{\text{min}}} \geq 5$  TeV. Thus, the fitting results can be considered as an evidence for possible transition from the hypothesis (ii) to (iii) at  $\sqrt{s} \gtrsim 5$  TeV. Undoubtedly, this transition imposes a small energy-dependence on the parameters involved in the fitting procedures, not considered here.

Furthermore the term  $\propto \varepsilon^{-1}$  should be negligibly small in parameterization for  $\sigma_{\text{tot}}^{xp}(s)$ ,  $x = p, \bar{p}$  (Table II) in order to get the validation of the Pomeranchuk theorem in both the classical formulation (11) and the generalized one (12).

Considering the condition  $a/\varepsilon \lesssim \delta$  for the energy range  $s \geq s_a$  as, at least, one of the possible signatures of the onset of the asymptotic energy region, one can assume that the model under consideration makes it possible to estimate  $s_a$  in order to magnitude. Here  $a \equiv |a_1| = |a_2|$  within uncertainties for certain data base, DB20 or DB201+, at fixed value of  $\sqrt{s_{\text{min}}} \geq 5$  TeV and  $\delta \ll 1$  mbarn is the empirical boundary. Taking into account the range  $a \sim (6.5 \times 10^7 - 1.7 \times 10^9)$  mbarn, which represents a variation of two orders in magnitude, and the choice  $\delta = 0.1$  mbarn, a small contribution coming from the non-logarithmic term, one can estimate  $\sqrt{s_a} \sim 25.5 - 130$  TeV. The lower value of the range for  $\sqrt{s_a}$  is close to the nominal energy of the high-energy LHC (HE-LHC) mode [38] while the upper one agrees quite reasonably with estimation deduced within approaches mentioned in Sec. II and III [23, 24]. Hopefully, this upper value can be achieved within newest option of the Future Circular Collider (FCC) project [39] with proton beam energy 75 TeV.

Of course, the above estimates for  $\sqrt{s_a}$  are rather rough, taking into account the wide range for the absolute values of  $a_{1,2}$  obtained with help of simultaneous fits in multi-TeV region  $\sqrt{s_{\text{min}}} \geq 5$  TeV (Table IV). Moreover, as stressed above, only experimental data for  $pp$  are approximated at  $\sqrt{s_{\text{min}}} \geq 5$  TeV. All of these allows only the preliminary statements at a qualitative level to be made regarding of the onset of the asymptotic energy domain.

The analytic functions deduced within various hypotheses (Table I, II) and numerical fit results (Table IV, VI) allow the phenomenological projections for the terms of the wide set  $\mathcal{G}$  of global scattering parameters and its derivative quantities, in particular, for energies  $\mathcal{O}(100)$  TeV and higher. The main features for such predictions are described in detail elsewhere [26, 34]. Simultaneous fit results obtained for database DB201+ (Table IV) allow predictions for the joined set  $\mathcal{G}$  since DB201+ is one of the most complete databases considered here and, on the other hand, this database satisfies the general requirements used in the formation of databases. To obtain estimates at (ultra-)high energies, it seems reasonable to use the fitted results for  $s_{\text{min}} \geq 1$  TeV<sup>2</sup>. Therefore predictions for the joined set  $\mathcal{G}$  are calculated and analyzed below, for  $\sqrt{s_{\text{min}}} = 1, 5$ , and 10 TeV. Calculations are performed for both collisions considered in the paper ( $pp, \bar{p}p$ ) for  $\sqrt{s} \geq 14$  TeV.

Within hypothesis (ii), the values of both the  $\sigma_{\text{tot}}^{xp}$  and  $\rho^{xp}$  do not depend on the type of collision for a given  $s_{\text{min}}$ , nor  $s_{\text{min}}$  indicated above for a fixed type of interaction within errors. The  $\rho^{xp}$  reaches the asymptotic level (22) within uncertainty at smallest  $\sqrt{s} = 14$  TeV under consideration at any  $s_{\text{min}}$ . Relative uncertainties for the estimations of  $\sigma_{\text{tot}}^{xp}$  ( $\delta_{\sigma}^{xp}$ ) are almost constant for all  $s_{\text{min}}$ , except for the highest  $\sqrt{s_{\text{min}}} = 10$  TeV, for which, after some decrease (increase), a fairly rapid transition to a constant level is observed at  $\sqrt{s} \approx 25$  (50) TeV for  $pp$  ( $\bar{p}p$ ) collisions. The

accuracy of estimates for  $pp$  is noticeably better than that for  $\bar{p}p$ , deteriorating for both collision types with increasing of  $s_{\min}$ , especially for transition from lower values of  $s_{\min}$  to the highest  $\sqrt{s_{\min}} = 10$  TeV under consideration. In the case of  $pp$  ( $\bar{p}p$ ), the values of  $\delta_{\sigma}^{xp}$  are at the level of 0.09 (0.22) at  $\sqrt{s_{\min}} = 1$  TeV, slightly increasing to 0.11 (0.27) at  $\sqrt{s_{\min}} = 5$  TeV. The decrease of  $\delta_{\sigma}^{pp}$  is observed from 0.17 to 0.15 at  $\sqrt{s} \gtrsim 25$  TeV, whereas there is a smooth increase of  $\delta_{\sigma}^{\bar{p}p}$  from 0.36 to a constant level of 0.38 at  $\sqrt{s} \gtrsim 50$  TeV at  $\sqrt{s_{\min}} = 10$  TeV. In the case of the  $\rho^{xp}$ , in general, a similar situation is observed for  $\delta_{\rho}^{xp}$  in the functional sense as well as for  $\delta_{\sigma}^{xp}$ : for  $pp$ , the  $\delta_{\rho}^{pp}$  quantity is approximately constant for all  $s_{\min}$  except for the  $\sqrt{s_{\min}} = 10$  TeV, for which the approach to the constant level is observed at  $\sqrt{s} \gtrsim 25$  TeV after some decrease of  $\delta_{\rho}^{pp}(s)$ ; for  $\bar{p}p$ , the  $\delta_{\rho}^{\bar{p}p}(s)$  agrees with constant quite well at lowest value  $\sqrt{s_{\min}} = 1$  TeV under discussion, and relative uncertainty  $\delta_{\rho}^{\bar{p}p}$  shows some increase for other  $s_{\min}$ , especially noticeable at highest  $\sqrt{s_{\min}} = 10$  TeV reaching a constant level at  $\sqrt{s} \gtrsim 50$  TeV. The relative uncertainties in projections of the  $\rho$ -parameter are smaller than those for the total cross section for any of the collision types considered here at any fixed  $s_{\min}$ . For  $pp$ , the  $\delta_{\rho}^{pp}(s)$  quantity agrees well with a constant 0.068 for  $\sqrt{s} \geq 14$  TeV at  $\sqrt{s_{\min}} = 1$  TeV whereas some decrease is observed for higher  $s_{\min}$ , especially for highest  $\sqrt{s_{\min}} = 10$  TeV. The  $\delta_{\rho}^{pp}(s)$  decreases with growth  $s$  from 0.106 (0.151) at  $\sqrt{s} = 14$  TeV down to the constant level 0.105 (0.133) at  $\sqrt{s} \geq 20$  (200) TeV for  $\sqrt{s_{\min}} = 5$  (10) TeV. The  $\delta_{\rho}^{\bar{p}p}(s)$  is approximately equal to the constant level 0.078 for  $\sqrt{s} \geq 14$  TeV at  $\sqrt{s_{\min}} = 1$  TeV and  $\delta_{\rho}^{\bar{p}p}$  increases from 0.082 (0.112) to a constant of 0.085 (0.127) at  $\sqrt{s} \gtrsim 30$  (150) TeV for  $\sqrt{s_{\min}} = 5$  (10) TeV. Thus, in the case of the  $\rho$ -parameter, the inverse energy dependence of the relative uncertainty is observed compared to that seen for the  $\sigma_{\text{tot}}^{xp}$  at  $\sqrt{s_{\min}} > 1$  TeV.

Estimates for each term of the set  $\mathcal{G}_1$ , calculated within the hypothesis (iii), are characterized by significantly better accuracy than those in the case of hypothesis (ii) for each of the  $s_{\min}$  used for the derivation of numerical estimates.

Within the hypothesis (iii), the values of the  $\sigma_{\text{tot}}^{xp}$  do not depend on the type of collision within the errors for a given  $s_{\min}$  as well as for the hypothesis (ii). However, in contrast to hypothesis (ii), some increase of estimations of  $\sigma_{\text{tot}}^{xp}$  at fixed  $s$  is observed with an increase in  $s_{\min}$ , especially in the transition from  $\sqrt{s_{\min}} = 1$  TeV to the highest  $\sqrt{s_{\min}} = 10$  TeV under consideration. The ratios of the estimates obtained for a fixed type of collision at given  $s$

and different  $s_{\min} - R_{\sigma,2/1}^{xp} \equiv \frac{\sigma_{\text{tot}}^{xp}(s)|_{s_{\min,2}}}{\sigma_{\text{tot}}^{xp}(s)|_{s_{\min,1}}} -$  reach constant levels with an increase in  $s$ , and this occurs, in general,

at the different  $s$  in dependence on both the  $s_{\min}$  and the collision type. The numerical values of these constant levels are  $\forall x = p, \bar{p} : R_{\sigma,2/1}^{xp} = 1.06 \pm 0.03, 1.16 \pm 0.07$  and  $1.09 \pm 0.07$  at  $\sqrt{s} \gtrsim 60, 50$  and  $40$  (60, 70 and 140) TeV in  $pp$  ( $\bar{p}p$ ) interactions for the pairs of lower boundary values for fitted ranges  $(\sqrt{s_{\min,1}}, \sqrt{s_{\min,2}}) = (1, 5), (1, 10)$  and  $(5, 10)$  in TeV, respectively. Thus the values of these constants with uncertainties do not depend either on the type of collision or the choice of the specific pair  $(s_{\min,1}, s_{\min,2})$ . The quantity  $\delta_{\sigma}^{xp}$  agrees quite well with constant at  $\sqrt{s} \geq 14$  TeV, and does not depend on the type of interaction for all  $s_{\min}$ , except for  $\sqrt{s_{\min}} = 10$  TeV, for which the onset of constant behavior is observed at  $\sqrt{s} \approx 100$  TeV after some decrease from 0.075 (0.065), at the smallest  $\sqrt{s} = 14$  TeV under consideration for  $pp$  ( $\bar{p}p$ ) collisions. The constant values for  $\delta_{\sigma}^{xp}$  are approximately 0.006, 0.024 and 0.061 at  $\sqrt{s_{\min}} = 1, 5$ , and 10 TeV, respectively. The quantity  $\delta_{\rho}^{xp}$  does not depend on the type of interaction and, due to the reasons indicated above in Sec. II, it becomes small, namely,  $< 10^{-4}$  already at  $\sqrt{s} \gtrsim 30, 125$ , and 350 TeV for  $\sqrt{s_{\min}} = 1, 5$ , and 10 TeV, respectively. Furthermore, the  $\delta_{\rho}^{xp}$  rapidly decreases with the increasing  $s$ . Therefore, within the framework of the hypothesis (iii), the  $\delta_{\rho}^{xp}$  can be taken equal to zero at  $\sqrt{s} \gtrsim 30, 125$ , and 350 TeV for  $\sqrt{s_{\min}} = 1, 5$ , and 10 TeV. Accounting for the aforementioned specific situation with the uncertainties for estimates of the  $\rho^{xp}$ -parameter, the median values of these estimates are only discussed below in this paragraph. The median values of the  $\rho$ -parameter are almost independent of the type of collision and coincide with the asymptotic level (22) with accuracy  $10^{-3}$  already at the smallest of the considered  $\sqrt{s} = 14$  TeV for  $\sqrt{s_{\min}} = 1$  TeV. There is no dependence on the  $\rho$ -parameter for the type of interaction, and the median values of  $\rho^{xp}$  coincide with  $\rho_a^{xp}$  (22) with accuracy  $10^{-3}$  at  $\sqrt{s} \gtrsim 50$  (100) TeV in the case of  $\sqrt{s_{\min}} = 5$  (10) TeV. The situation for the ratio of estimates of  $\rho$

obtained for a fixed type of interaction at given  $s$  and different  $s_{\min} - R_{\rho,2/1}^{xp} \equiv \frac{\rho^{xp}(s)|_{s_{\min,2}}}{\rho^{xp}(s)|_{s_{\min,1}}} -$  in general, is similar

to that observed for  $\sigma_{\text{tot}}^{xp}$ . But, unlike on total cross sections,  $\forall x = p, \bar{p} : R_{\rho,2/1}^{xp}$  agree with unity with high accuracy better than  $7 \times 10^{-4}$  at  $\sqrt{s} \geq 100$  TeV for any pair  $(s_{\min,1}, s_{\min,2})$  considered here.

The detailed analysis made above for the predictions for the terms of the set  $\mathcal{G}_1$  unambiguously indicates that the terms  $\Delta_{\text{tot}}$  and  $R_{\text{tot}}^{\bar{p}/p}$  of the set  $\mathcal{G}_2$  coincide with their asymptotic values (11) and (12) within the uncertainties at  $\sqrt{s} \geq 14$  TeV for both hypotheses (ii) and (iii), at any  $s_{\min} \geq 1$  TeV<sup>2</sup>. The smooth increase is observed for  $\sigma_{\text{tot}}^{xp}$  with the growth of  $s$  for any  $s_{\min}$ . Therefore, one can conclude that the realization of the scenario according to the Pomernichuk theorem (12) seems more preferable at asymptotic energies than the scenario with the formulation (11) for any hypotheses discussed in this paper.

Furthermore, the aforementioned study of energy behavior of projections for the terms of the joined ensemble  $\mathcal{G}$



TABLE VII: Predictions for  $pp$  based on the simultaneous fit of  $\mathcal{G}_1$  for DB20<sub>1</sub>+ at  $\sqrt{s_{\min}} = 5$  TeV with first / second line in the cell for the hypothesis (ii) / (iii).

Parameter	$\sqrt{s}$ , TeV									
	(HL-)LHC, HE-LHC, LHC-ultimate				SPPC, FCC-hh, VLHC-I, II					
	14	27	42	40	70.6	100	125	150	175	
$\sigma_{\text{tot}}^{pp}$ , mbarn	$108 \pm 12$	$117 \pm 13$	$122 \pm 13$	$122 \pm 13$	$128 \pm 14$	$132 \pm 14$	$135 \pm 14$	$137 \pm 15$	$139 \pm 15$	
	$108.5 \pm 2.7$	$117.3 \pm 2.8$	$122.7 \pm 2.9$	$122.1 \pm 2.9$	$129 \pm 3$	$133 \pm 3$	$135 \pm 3$	$138 \pm 3$	$139 \pm 3$	
$\rho^{pp} \times 10^3$	$87 \pm 9$	$80 \pm 8$	$77 \pm 8$	$77 \pm 8$	$73 \pm 8$	$71 \pm 7$	$69 \pm 7$	$68 \pm 7$	$67 \pm 7$	
	$83.6 \pm 0.4$	$77.3 \pm 0.1$	$73.89 \pm 0.03$	$74.24 \pm 0.04$	$70.38 \pm 0.01$	$68.24 \pm 0.01$	66.93	65.91	65.06	
	VLHC-II		ultra-high energy cosmic rays					higher energies		
	200	110	170	250	500	750	$10^3$	$5 \times 10^3$	$10^4$	
$\sigma_{\text{tot}}^{pp}$ , mbarn	$140 \pm 15$	$133 \pm 14$	$138 \pm 15$	$143 \pm 15$	$151 \pm 16$	$155 \pm 17$	$159 \pm 17$	$172 \pm 19$	$185 \pm 20$	
	$141 \pm 3$	$134 \pm 3$	$139 \pm 3$	$143 \pm 3$	$151 \pm 4$	$156 \pm 4$	$159 \pm 4$	$178 \pm 4$	$186 \pm 4$	
$\rho^{pp} \times 10^3$	$67 \pm 7$	$70 \pm 7$	$68 \pm 7$	$66 \pm 7$	$62 \pm 7$	$60 \pm 6$	$59 \pm 6$	$53 \pm 6$	$51 \pm 5$	
	64.35	67.67	65.22	63.19	59.85	58.06	56.85	50.92	48.73	

shows that, in general, physical quantities and their uncertainties reach corresponding asymptotic or constant levels at energies  $\mathcal{O}(100 \text{ TeV})$ . That can be considered as indirect evidence in favor of the range for  $\sqrt{s_a}$ , derived with help of the condition for  $a/\varepsilon$ .

Some numerical values for estimates of global scattering parameters are shown in Table VII for  $pp$  in the energy range from the nominal  $\sqrt{s}$  of the LHC up to the high boundary of the PeV domain  $\sqrt{s} = 10 \text{ PeV}$  based on the detailed analysis above and the reasons discussed elsewhere [26, 34]. The fitted results for DB20<sub>1</sub>+ at  $\sqrt{s_{\min}} = 5 \text{ TeV}$  are used to calculate the estimates of terms of the set  $\mathcal{G}_1$ . The choice of the value  $\sqrt{s_{\min}} = 5 \text{ TeV}$  for Table VII is based on the detailed analysis in subsec. IV A as well as in the present section. In particular, the simultaneous fit for  $\mathcal{G}_1$  at that  $s_{\min}$  is characterized firstly by enough number of experimental points in fitted sample together with statistically acceptable  $\chi^2/\text{n.d.f.}$  in difference with smaller  $s_{\min}$  and, secondly, by the higher robustness of fit results in comparison with the  $\sqrt{s_{\min}} = 10 \text{ TeV}$ . As seen from Table VII, the predictions for  $\sigma_{\text{tot}}^{pp}$  and  $\rho^{pp}$  coincide within the uncertainties for various hypotheses under consideration. Direct comparison is impossible for the results in Table VII and the projections within AQFT [26] because of noticeably different  $s_{\min}$  used for simultaneous fits and, consequently, for calculations of estimates for  $\sigma_{\text{tot}}^{pp}$  and  $\rho^{pp}$ . Nevertheless, accounting for this feature, one can observe the following: the estimates obtained within the present work are characterized much better precision than those within AQFT [26], especially for  $\rho$ -parameter; the estimates mostly agree within uncertainties for two approaches for any global scattering parameters under discussion, except for of  $\sigma_{\text{tot}}^{pp}$  at ultra-high energies  $\sqrt{s} \geq 5 \text{ PeV}$ . In general, this discrepancy can be expected since the present approach provides  $\sigma_{\text{tot}}^{pp} \propto \ln \varepsilon$  at  $s \rightarrow \infty$ , i.e. the slowest increase of the total cross section at (ultra-)high energies, and this functional form for  $\sigma_{\text{tot}}^{pp}$  should lead to the continuously increasing difference with results of AQFT with the growth of  $s$ .

## VI. CONCLUSION

The asymptotic behavior of the wide set  $\mathcal{G}$  of scattering parameters is studied with the help of crossing property, the DDR and the optical theorem in  $pp$  and  $\bar{p}p$  collisions. It is important to point out that we obtained an intercept  $\alpha_{\mathbb{P}} = 1$ , typical of a soft Pomeron (low momentum transfer). This is a consequence of the use of the first-order approximation for the DDR. In contrast, the introduction of higher derivative orders to describe the dispersion relation may introduce subleading contributions at high energies, which can lead to a Pomeron intercept different from 1. The simplest functional form for the real part of the forward scattering amplitude is used for the asymptotic energy domain to deduce the analytic expressions for  $\sigma_{\text{tot}}^{xp}$  and  $\rho^{xp}$ ,  $x = p, \bar{p}$  as well as for some combinations of total cross sections, which are important for verification of the Pomeranchuk theorem. Within that form, for  $\text{Re}F_{xp}$ , the two hypotheses – (ii) and (iii) – are kept with non-zero constants for  $\text{Re}F_{xp}$  at asymptotic energies.

Three consequent stages are considered for the most current database for global scattering parameters in elastic  $pp$  and  $\bar{p}p$  scattering, namely, the latest PDG sample (DB20) and all available experimental results (DB20<sub>1</sub>+, DB20<sub>2</sub>+). The analytic parameterizations deduced considering both hypotheses provide a quantitative description of energy-dependence of measured global scattering parameters – set  $\mathcal{G}_1$  – with mostly robust values of fit parameters for any

DBs. The fit qualities are reasonable for energy range  $\sqrt{s} \geq 0.06$  TeV, and the quantity is statistically acceptable at the low boundary for fit domain  $\sqrt{s_{\min}} \geq 0.1$  TeV for hypothesis (ii). The corresponding ranges are significantly shifted to the higher energies and they are  $\sqrt{s} \geq 0.5$  TeV and  $\sqrt{s} \geq 1$  TeV for statistically reasonable and acceptable quantities, respectively, for hypothesis (iii) due to its "extremely" asymptotic nature. Detailed analysis of accelerator data only shows that hypotheses (ii) and (iii) allow the qualitative description for these data up to the  $\sqrt{s_{\min}} = 5$  TeV. The experimental database created for some interrelations between  $\sigma_{\text{tot}}^{pp}$  and  $\sigma_{\text{tot}}^{pp}$  – set  $\mathcal{G}_2$  – covers the energy domain  $\sqrt{s} < 0.5$  TeV only and most of the points are at  $\sqrt{s} \lesssim 0.06$  TeV. The analytic expressions deduced for terms of the set  $\mathcal{G}_2$  within hypotheses (ii) and (iii) only provide a qualitative description of the energy dependence of these terms at  $\sqrt{s_{\min}} \geq 0.04$  TeV. In general, such relation between simultaneous fits and data is expected since the formulas for the terms of the set  $\mathcal{G}_2$ , as well as for the set  $\mathcal{G}_1$ , are asymptotic for both hypotheses under study. Nevertheless, the consideration of the joined ensemble  $\mathcal{G}$  indicates that, in general, one can obtain the smooth energy-dependence for the terms of  $\mathcal{G}_1$  in multi-TeV range with the help of the fit results for  $\mathcal{G}_2$  at much smaller collision energies, and the calculated curves for  $\mathcal{G}_1$  agree with both the experimental data and the corresponding fitted curves, at least, reasonably.

Study of empirical conditions for the functional forms of the analytic expressions for measured global scattering parameters allows the following rough estimation of collision energy for the onset of the asymptotic region  $\sqrt{s_a} \sim 25.5 - 130$  TeV.

Based on the simultaneous fit results, the estimations are calculated for the total cross section and the  $\rho$ -parameter, considering the elastic  $pp$  scattering at different  $s$ , up to energy frontier  $\sqrt{s} = 10$  PeV. These estimations with uncertainties are robust for various  $\sqrt{s_{\min}} \geq 1$  TeV and types of collisions. The numerical values of the estimations for  $\sigma_{\text{tot}}^{pp}$  and  $\rho^{pp}$  obtained with the help of the simultaneous fit of  $\mathcal{G}_1$  for DB201+ at  $\sqrt{s_{\min}} = 5$  TeV agree for hypothesis (ii) and (iii) within the errors. The estimations for  $\sigma_{\text{tot}}^{pp}$  can be considered conservative due to functional form for this quantity at (ultra-)high energies which consequently leads to a slow increase of  $\sigma_{\text{tot}}^{pp}$  as  $s$  rise. Detailed analysis of the predictions for terms of the joined ensemble  $\mathcal{G}$  unambiguously indicates that the realization of the scenario with the generalized formulation of the Pomeranchuk theorem seems more suitable at asymptotic energies than the scenario with the original formulation of this theorem, for any hypotheses discussed along the paper. The aforementioned study shows that, in general, physical quantities and their uncertainties reach corresponding asymptotic or constant levels at energies  $\mathcal{O}(100 \text{ TeV})$ . As commented before, it can be considered an indirect indication to support the range for  $\sqrt{s_a}$ , obtained by considering the empirical conditions described in this work.

As a last comment, it is important to stress that at very high energies, possible non-linearities on the elastic forward quantities may be taken into account by using higher-order derivative terms in the dispersion relations. This procedure may lead to corrections on the results presented here. This question is presently under study and will be published elsewhere.

### Acknowledgments

SDC thanks to UFSCar for the financial support. The work of V.A.O. was supported partly by NRNU MEPhI Program "Priority 2030".

- 
- [1] M. Froissart, Phys. Rev. **123**, 1053 (1961).
  - [2] A. Martin, II Nuovo Cim. **A42**, 930 (1966).
  - [3] A. Martin, Nuovo Cim. **A44**, 1219 (1966).
  - [4] L. Lukaszuk and A. Martin. Nuovo Cim. **A52**, 122 (1967).
  - [5] A. Martin, Phys. Rev. **D80**, 065013 (2009).
  - [6] O. Nachtmann, Ann. Phys. **209**, 436 (1991).
  - [7] I. Y. Pomeranchuk. JETP **7**, 499 (1958).
  - [8] S. D. Campos, Chin. Phys. **C44**, 103103 (2020).
  - [9] F. E. Low, Phys. Rev. **D12**, 163 (1975).
  - [10] S. Nussinov, Phys. Rev. Lett. **34**, 1286 (1975).
  - [11] R. J. Eden, P. V. Landshoff, D. I. Olive and J. C. Polkinghorne, *The Analytic S-Matrix*. Cambridge Univ. Press (1966).
  - [12] R. F. Ávila, S. D. Campos, M. J. Menon and J. Montanha, Eur. Phys. J. **C47**, 171 (2006).
  - [13] P. D. B. Collins and E. J. Squires, *Regge poles in particle physics*. Springer tracts in modern physics, **45**. Springer-Verlag (1968).
  - [14] R. F. Ávila and M. J. Menon, Nucl. Phys. **A744**, 249 (2004).

- [15] A. Donnachie, H. G. Dosch, P. V. Landshoff and O. Nachtmann, *Pomeron physics and QCD*. Cambridge Univ. Press (2002).
- [16] P.A. Zyla *et al.* (Particle Data Group), Prog. Theor. Exp. Phys. **2020**, 083C01 (2020).
- [17] T. Kinoshita, J. J. Loeffel and A. Martin, Phys. Rev. Lett. **10**, 460 (1963).
- [18] R. J. Eden, Phys. Rev. Lett. **16**, 39 (1966).
- [19] T. Kinoshita, in: *Perspectives in Modern Physics*, Ed. R. E. Marshak. p. 211. Wiley, New York (1966).
- [20] G. Grunberg and Tran N. Truong, Phys. Rev. Lett. **31**, 63 (1973); Phys. Rev. D **9**, 2874 (1974).
- [21] D. A. Fagundes, A. Grau, G. Pancheri, O. Shekhovtsova and Y. N. Srivastava, Phys. Rev. D **96**, 054010 (2017).
- [22] E. Leader and E. Predazzi, *An intriduction to gauge theories and modern particle physics*. Vol. **2**. Cambridge Univ. Press (1996).
- [23] V. A. Petrov and V. A. Okorokov, Int. J. Mod. Phys. A **33**, 1850077 (2018).
- [24] V. A. Okorokov, Phys. At. Nucl. **81**, 508 (2018).
- [25] S. D. Campos and V. A. Okorokov, Int. J. Mod. Phys. A **25**, 5333 (2010).
- [26] V. A. Okorokov and S. D. Campos, Int. J. Mod. Phys. A **32**, 1750175 (2017).
- [27] J. Adam *et al.* (STAR Collaboration), Phys. Lett. C **808**, 135663 (2020).
- [28] G. Antchev *et al.* (TOTEM Collaboration), Eur. Phys. J. C **79**, 785 (2019).
- [29] V. A. Okorokov, Adv. High Energy Phys. **2015**, 914170 (2015); the database for the forward slope is available at arXiv: 1501.01142 [hep-ph] (2015).
- [30] V. A. Okorokov, Int. J. Mod. Phys. A **27**, 1250037 (2012).
- [31] V. A. Okorokov, Adv. High Energy Phys. **2015**, 790646 (2015); *ibid* **2016**, 5972709 (2016); *ibid* **2017**, 5465398 (2017).
- [32] M. M. Block and R. N. Cahn, Phys. Lett. B **149**, 245 (1984); Rev. Mod. Phys. **57**, 563 (1985).
- [33] T. T. Chou and C. N. Yang, Phys. Rev. **170**, 1591 (1968); Phys. Lett. B **128**, 457 (1983).
- [34] V. A. Okorokov, Phys. At. Nucl. **82**, 134 (2019).
- [35] V. V. Anisovich, Phys. Usp. **185**, 963 (2015).
- [36] R.U. Abbasi *et al.* (Telescope Array Collaboration), Phys. Rev. D **92**, 032007 (2015).
- [37] P. Abreu *et al.* (The Pierre Auger Collaboration), Phys. Rev. Lett. **109**, 062002 (2012).
- [38] A. Abada *et al.*, Eur. Phys. J. Special Topics **228**, 1109 (2019).
- [39] A. Abada *et al.*, Eur. Phys. J. Special Topics **228**, 755 (2019).

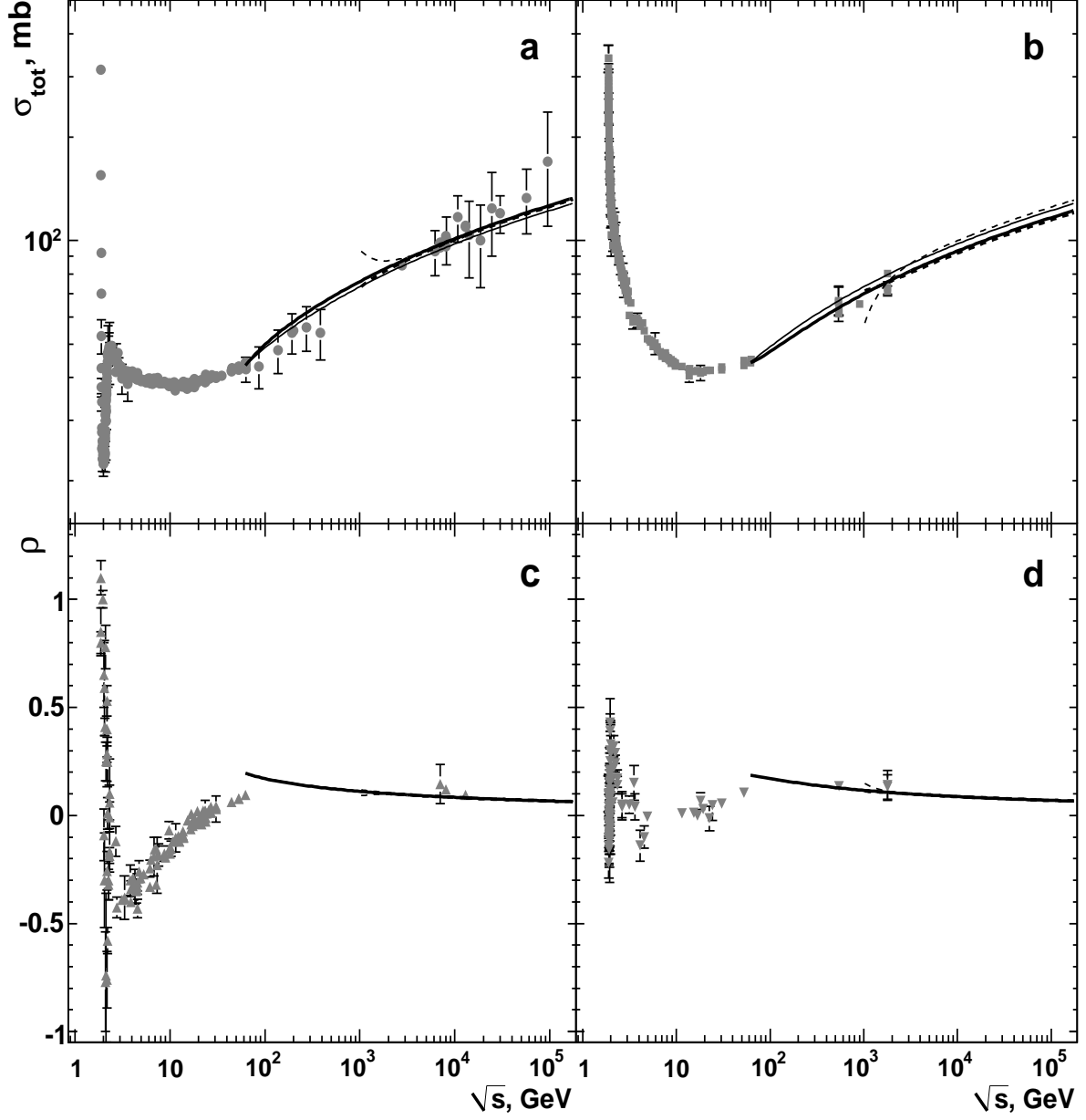


FIG. 1: The energy dependence of the measurements for the terms of  $\mathcal{G}_1$  and results of simultaneous fits of all these terms. Experimental results are from the DB20<sub>1</sub>+. The solid lines correspond to the fit at  $\sqrt{s_{\text{min}}} = 0.06$  TeV, the dashed lines are at  $\sqrt{s_{\text{min}}} = 1$  TeV. The thick lines show the fit curves for the hypothesis (ii) and the other lines correspond to the hypothesis (iii).

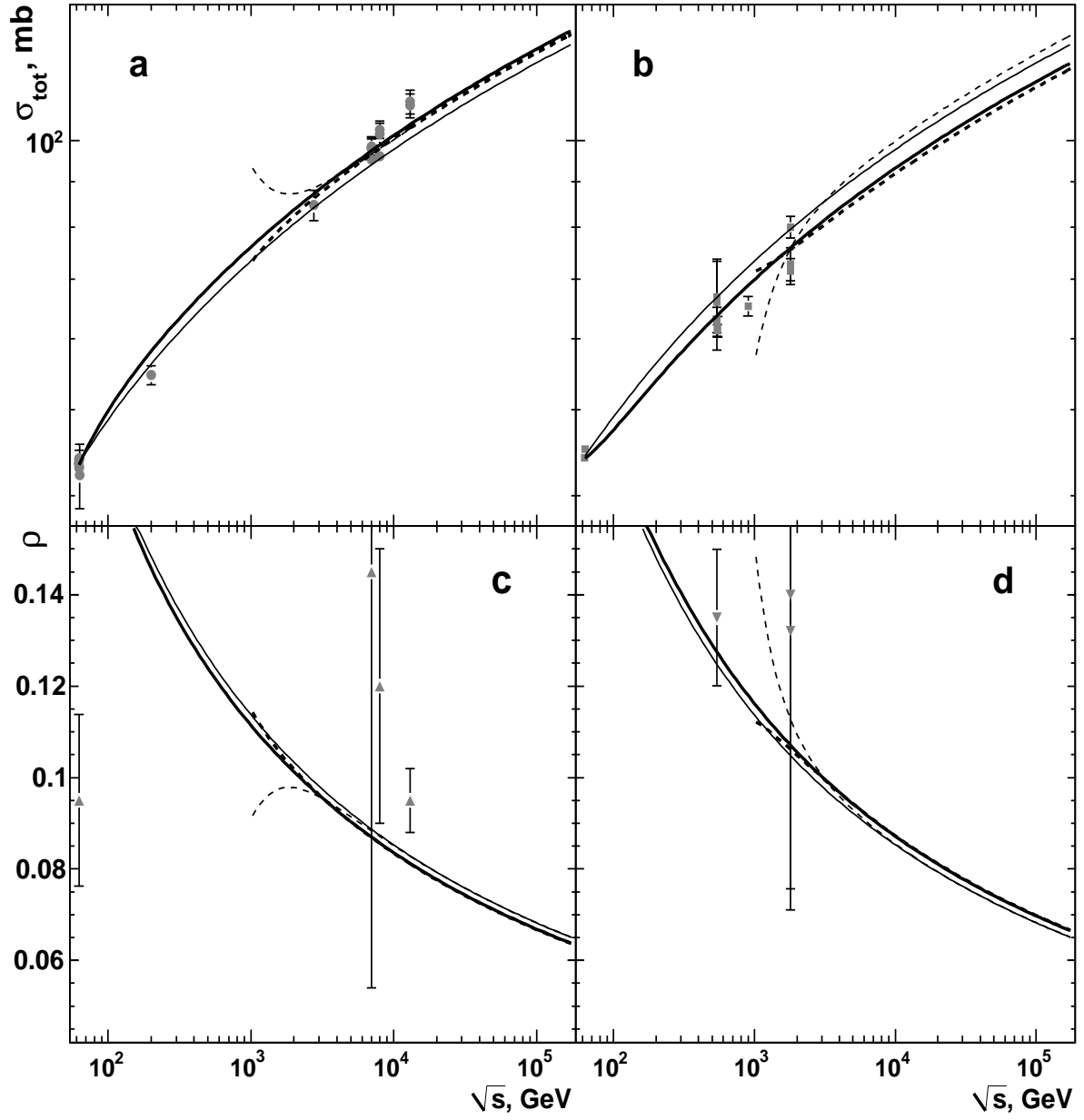


FIG. 2: The comparison of the data from accelerator experiments for the terms of  $\mathcal{G}_1$  and approximating curves from simultaneous fits of all these terms at  $\sqrt{s} \geq 0.06$  TeV. Experimental results are from the subsample DB<sub>ac</sub>20<sub>1</sub>+. The notations for the curves and experimental data base are identical to that in Fig. 1.

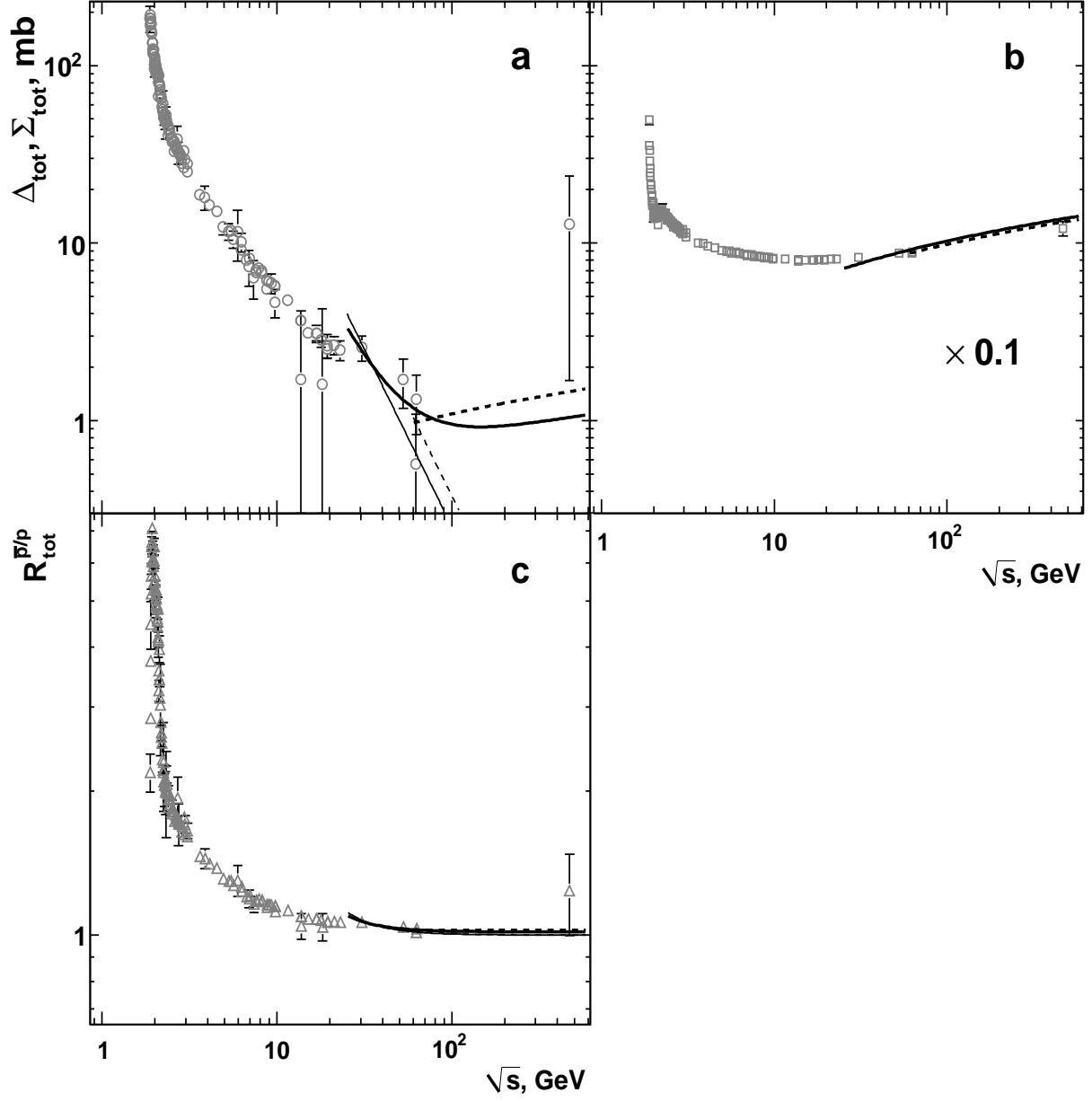


FIG. 3: The energy dependence of the measurements for the terms of  $\mathcal{G}_2$  and results of simultaneous fits of all these terms. Points are calculated with help of the experimental results from the DB20. The point values and fit curves are multiplied on 0.1 for  $\Sigma_{\text{tot}}$  (b). The solid lines correspond to the fit at  $\sqrt{s_{\text{min}}} = 0.03$  TeV, the dashed lines are at  $\sqrt{s_{\text{min}}} = 0.06$  TeV. The thick lines show the fit curves for the hypothesis (ii) and two other lines correspond to the hypothesis (iii).



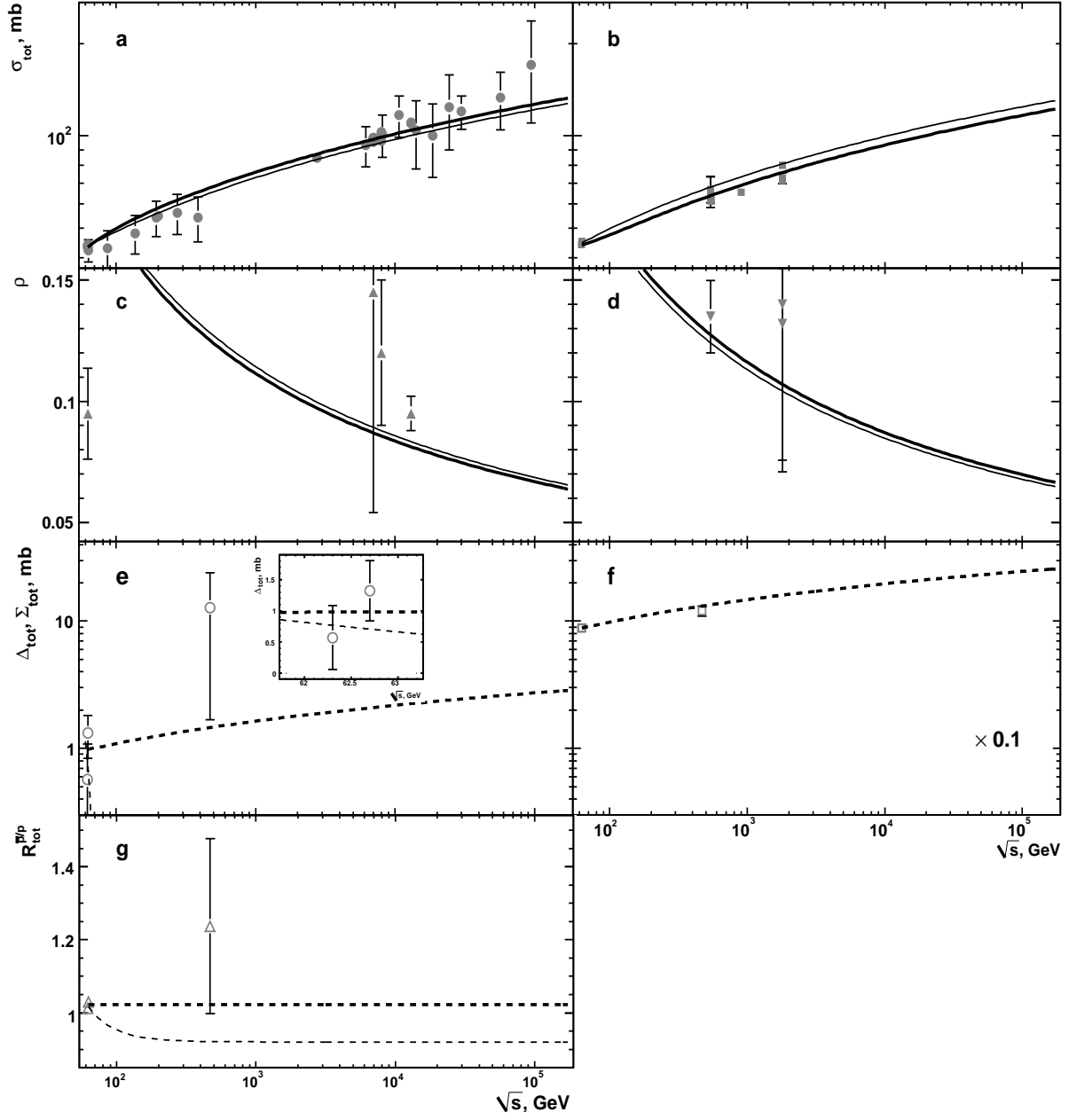


FIG. 4: The energy dependence for the terms of the joined set  $\mathcal{G}$  and curves obtained with help of the results shown in Table IV for the database DB20<sub>1</sub>+ and in Table VI within hypothesis (ii). The experimental results and curves are shown at  $\sqrt{s} \geq 0.06$  TeV. The inner panel for  $\Delta_{\text{tot}}$  (e) shows the narrow energy range close to the  $\sqrt{s} = 62.5$  GeV. The point values and curves are multiplied on 0.1 for  $\Sigma_{\text{tot}}$  (f). The solid lines correspond to the curves for the terms of  $\mathcal{G}_1$ , dashed lines are for  $\mathcal{G}_2$ . The thick curves are from the simultaneous fit results for the corresponding  $\mathcal{G}_i$ ,  $i = 1, 2$ ; the thin lines are calculated with help of the values of free parameters obtained from the simultaneous fit of the terms of the adjoint set, i.e. the curves for the terms of  $\mathcal{G}_1$  are calculated with the free parameter values obtained for  $\mathcal{G}_2$  by the simultaneous fit at  $\sqrt{s_{\text{min}}} = 0.06$  TeV and vice versa.

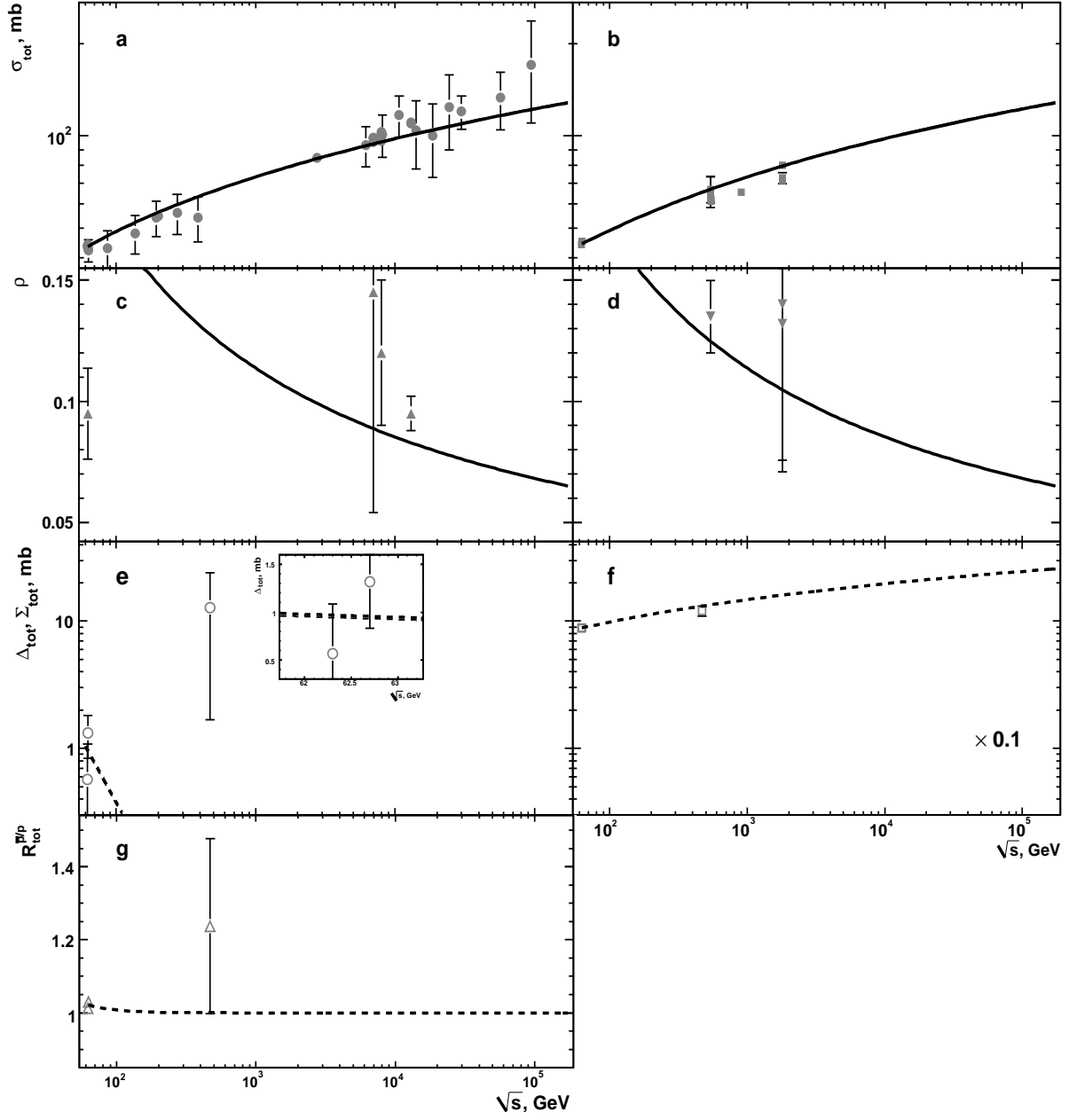


FIG. 5: The energy dependence for the terms of the joined set  $\mathcal{G}$  and curves obtained with help of the results shown in Table IV for the database DB20<sub>1</sub>+ and in Table VI within hypothesis (iii). The experimental results and curves are shown at  $\sqrt{s} \geq 0.06$  TeV. The inner panel for  $\Delta_{\text{tot}}$  (e) shows the narrow energy range close to the  $\sqrt{s} = 62.5$  GeV. The point values and curves are multiplied on 0.1 for  $\Sigma_{\text{tot}}$  (f). The solid lines correspond to the curves for the terms of  $\mathcal{G}_1$ , dashed lines are for  $\mathcal{G}_2$ . The thick curves are from the simultaneous fit results for the corresponding  $\mathcal{G}_i$ ,  $i = 1, 2$ ; the thin lines are calculated with help of the values of free parameters obtained from the simultaneous fit of the terms of the adjoint set, i.e. the curves for the terms of  $\mathcal{G}_1$  are calculated with the free parameter values obtained for  $\mathcal{G}_2$  by the simultaneous fit at  $\sqrt{s_{\text{min}}} = 0.06$  TeV and vice versa.